in silico Plants Vol. 4, No. 1, pp. 1–21
https://doi.org/10.1093/insilicoplants/diac004
Advance Access publication 14 April 2022
Original Research

in silico Plants
OXFORD

A conserved cellular mechanism for cotton fibre diameter and length control

Makato Yanagisawa[1,5], Sedighe Keynia[2], Samuel Belteton[1,3], Joseph A. Turner[2] and Daniel Szymanski[1,4,*]

[1]Department of Botany and Plant Pathology, Purdue University, West Lafayette, Indiana, USA
[2]Mechanical and Materials Engineering, University of Nebraska–Lincoln, Lincoln, Nebraska, USA
[3]Microscopy Imaging Core Suite, New Mexico State University, Las Cruces, New Mexico, USA
[4]Department of Biological Sciences, Purdue University, West Lafayette, Indiana, USA
[5]Present address: Division of Cell Fate Dynamics and Therapeutics, Department of Biosystems Science, Institute for Frontier Life and Medical Sciences, Kyoto University, Kyoto, Japan
M.Y. and S.K. should be considered joint first authors.

Guest Editor: Tsu-Wei Chen

Editor-in-Chief: Stephen P Long

*Corresponding author's e-mail address: szymandb@purdue.edu

ABSTRACT

Highly polarized cotton fibre cells that develop from the seed coat surface are the foundation of a multi-billion-dollar international textile industry. The unicellular trichoblast emerges as a hemispherical bulge that is efficiently converted to a narrower and elongated shape that extends for about 2 weeks before transitioning into a cellulose-generating machine. The polarized elongation phase employs an evolutionarily conserved microtubule-cellulose synthase control module that patterns the cell wall and enables highly anisotropic diffuse growth. As the multi-scale interactions and feedback controls among cytoskeletal systems, morphologically potent cell wall properties, and a changing cell geometry are uncovered, opportunities emerge to engineer architectural traits. However, in cotton, such efforts are hampered by insufficient knowledge about the underlying control mechanisms. For example, fibre diameter is an important trait that is determined during the earliest stages of development, but the basic growth mode and the mechanisms by which cytoskeletal and cell wall systems mediate fibre tapering are not known. This paper combines multiparametric and multiscale fibre phenotyping and finite element computational modelling of a growing cell to discover an evolutionarily conserved tapering mechanism. The actin network interconverts between two distinct longitudinal organizations that broadly distributes organelles and likely enables matrix secretion patterns that maintain cell wall thickness during growth. Based on plausible finite element models and quantitative analyses of the microtubule cytoskeleton, tapering and anisotropic growth is programmed by a constricting apical microtubule depletion zone and highly aligned microtubules along the fibre shaft. The finite element model points to a central role for tensile forces in the cell wall to dictate the densities and orientations of morphologically potent microtubules that pattern the cell wall.

KEYWORDS: Biomechanics; cell morphogenesis; cellulose; cytoskeleton; cotton fibre; finite element modelling; mechanosensing.

1. INTRODUCTION

Rational design of plant traits via combinations of breeding and genetic engineering strategies is a great challenge in modern agriculture. Computational simulation and systems-level biology can enable rapid progress, but model validation is often challenging due to limitations associated with in vivo experiments. However, the simulation process forces investigators to reduce the complexity of the problem to its most salient components and to develop measurement strategies

to validate input parameters. Realistic simulations let the major regulatory components be studied in order to identify and predict which variables might have the strongest effect. For example, analyses of the importance of photosynthetic efficiency in crop yield provide several excellent examples showing how particular biochemical pathways, cell morphologies and canopy architectures contribute to photosynthetic efficiency (Horton 2000). This work led to successful engineering of metabolic pathways that both increase biomass accumulation and improve nitrogen economy. Recent finite element modelling (FEM) of plant cells, tissues and organs has highlighted the potential of such models to guide experimental analysis of growth control across wide spatial scales (Hamant *et al.* 2008; Prusinkiewicz and Runions 2012; Bassel *et al.* 2014; Boudon *et al.* 2015; Yanagisawa *et al.* 2015; Evers 2016; Kierzkowski *et al.* 2019). This paper leverages the single cell system of cotton fibre development and combines imaging and mechanical simulations of the growth process to predict key parameters that control the fibre tapering and growth pattern.

Cotton fibres or trichomes are remarkable polarized cells that emerge from the surface of the developing seed coat. At the time of anthesis, more than 10,000 cells per ovule execute a fairly synchronized and predictable program of primary cell wall elongation, secondary cell wall thickening and maturation (Stewart 1975; Applequist *et al.* 2001; Haigler *et al.* 2012). The result is a long, twisted fibre that is the foundation of a global textile industry. As with many important crop plants, commercially important modern varieties were derived from domestication and improvement processes that trace back thousands of years (Wendel *et al.* 1989; Wendel and Cronn 2003; Wendel *et al.* 2010; Renny-Byfield *et al.* 2015), all motivated by desirable mechanical properties of the readily harvestable, single-celled, epidermal seed hairs. As a result, modern high-yielding annualized crop plants have relatively long and strong fibres (up to 5 cm). Recently, it has been shown that a key determinant of fibre twisting resides in the post-translational control of a cotton orthologue of the known microtubule binding protein SPIRAL1 (Zang *et al.* 2021), pointing to a critical role for a fine-tuned microtubule-cellulose system during fibre morphogenesis. Given the advances in cell and systems biology and the mechanical modelling of cells (Fayant *et al.* 2010; Yanagisawa *et al.* 2015; Belteton *et al.* 2021), there are many opportunities to discover and manipulate the cellular determinants of fibre quality.

The dynamics of plant growth are inherently connected with the mechanical behaviour of the cell wall. Turgor pressure driven cell wall-stress, the resulting strain in the wall matrix, continued cell wall synthesis, and cell wall modifications collectively govern the patterns of cell and tissue cell expansion (Szymanski and Cosgrove 2009). Quantitative analysis of cell growth often necessitates the use of numerical approaches to uncover these important relations(Lockhart 1965; Smithers *et al.* 2019). The complex geometry and boundary conditions of plant cells and organs often necessitate simplifying assumptions, but appropriate sensitivity studies can quantify the impact of any assumptions made. In this way, the combination of experimental data and computational modelling can often lead to new insights into cell morphogenesis (Fayant *et al.* 2010; Forouzesh *et al.* 2013; Yanagisawa *et al.* 2015; Belteton *et al.* 2021; Keynia *et al.* 2022).

Because fibres grow on the outside of ovules that are readily harvested and imaged, the cotton fibre is a powerful single cell model for insight into plant growth and development, primary wall assembly and cell morphogenesis (Triplett 2000; Haigler *et al.* 2012). Swollen fibre at early stages of development rapidly taper to acquire a cell diameter (Applequist *et al.* 2001; Stiff and Haigler 2016), and this shape is maintained during an extended phase of rapid elongation that persists until ~16 days post anthesis (DPA). During the subsequent transition to secondary cell wall synthesis, fibre elongation slows until the fibre reaches its final length and converts completely to thickening a cellulose rich wall and eventual cell death (Meinert and Delmer 1977; Seagull 1990). Cellular pathways that control the rate and duration of fibre elongation as well as those that impact material properties of the cell wall are potential targets for crop improvement.

Fibre shape is programmed indirectly by the microtubule and actin cytoskeletons. These cytoskeletal systems function together to organize the cytoplasm and pattern the cellulose and matrix components that determine cellular growth patterns (Baskin 2005; Szymanski and Cosgrove 2009; Yanagisawa *et al.* 2015). Young cotton fibres have a dense microtubule array, depolymerization of which causes isotropic swelling (Seagull 1990, 1992; Tiwari and Wilkins 1995) an outcome that can be explained by the mechanical organization of the cell wall, in which microtubules pattern parallel cellulose microfibrils (Seagull 1992; Paredez *et al.* 2006; Li *et al.* 2012; Yanagisawa *et al.* 2015). In *Arabidopsis* leaf trichomes, another aerial trichoblast analogous to cotton fibres, there is a clear threshold requirement for transverse microtubule alignment to generate anisotropic diffuse growth and cells with extreme aspect ratio (Yanagisawa *et al.* 2015). Along similar lines, a wide variety of genetic and cell biology data point to a central importance of the actin cytoskeleton during fibre morphogenesis. The actin bundle network provides tracks for long distance intracellular transport of cell wall matrix, and disruption of the actin by either inhibitors or mutations causes fibre swelling, reduced cell elongation and defective cell tapering (Seagull 1990; Li *et al.* 2005). Further, actin cytoskeleton genes are repeatedly correlated with fibre quality in gene expression profiling experiments (Bao *et al.* 2011a; Chen *et al.* 2012; Hu *et al.* 2014; Yoo and Wendel 2014).

Fibre diameter is a valuable trait, because all other properties being equal, lower diameter means a higher thread count and a soft silky feel, and a premium price for producers (Kelly *et al.*, 2015). Fibre diameter varies among cotton species and is defined at an early stage of fibre development (Applequist *et al.* 2001; Stiff and Haigler 2016; Graham and Haigler 2021); however, it has not been recognized as a distinct developmental stage in previous reviews on this topic (Kim and Triplett 2001b; Qin and Zhu 2011). The cellular mechanism of trichoblast tapering has been deciphered in Arabidopsis leaf hairs (Yanagisawa *et al.* 2015), and the cytoskeletal patterns and growth behaviours of tapering leaf hairs and cotton fibres are quite similar (Yanagisawa *et al.* 2018). Multivariate live cell imaging and finite element modelling were used to demonstrate that leaf hairs have specific threshold requirements for microtubule and microfibril alignment that is required for highly anisotropic cell expansion without radial swelling (Yanagisawa *et al.* 2015). Interestingly, tapering is mediated by the progressive restriction of an apical microtubule-depletion-zone (MDZ) and the corresponding apical patch of isotropic cell wall (Yanagisawa *et al.* 2015). The MDZ is also an important region for cell signalling where a well-characterized actin polymerization module organizes intracellular trafficking patterns at cellular scales (Basu *et al.* 2008; Yanagisawa *et al.* 2015; Yanagisawa *et al.* 2018). Early-stage

cotton fibres have an MDZ; however, its role and the general role of microtubule-microfibril patterning during the earliest phases of fibre morphogenesis are not known.

In this paper, multi-scale examinations of the cotton fibre cell wall behaviours, cytoskeleton organizations and cell shape change patterns were conducted as a function of the fibre tapering. These experiments identified differences between cotton fibres and leaf hairs in the organization of the actin network; however, there were strong similarities between the microtubule systems in these cell types. Quantitative data on shape change patterns, subcellular strain gradients, cell wall thickness and microtubule alignment were used to parameterize and validate a full 3D FE growth model of a tapering cotton fibre. The model predicts strict requirements for the degree and location of aligned cellulose microfibrils along the cell shaft. The model is based on a multi-layered, viscoelastic, composite cell wall and demonstrates the plausibility of a tapering mechanism in which an apical isotropic patch at the cell tip becomes progressively constricted until the cell reaches its final diameter. These results provide a solid foundation to develop strategies to engineer the important trait of cotton fibre diameter.

2. MATERIAL AND METHODS

2.1 Cotton cultivars and growth conditions

Gossypium barbadense cv. PhytoGen 800 and *Gossipium hirsutum* cv. Delta Phe90 plants were grown in a greenhouse under ~16/8 day/night cycle at 28 °C in a 50:50 mixture of Promix FLX soil and Sungro coarse perlite premium grade (Carl Brehob and Sons, Indianapolis, IN) in 14 inch diameter 7 gallon Classic 2800 pots (Hummert International, Earth City, MO) with holes in the bottom. Plants were fertilized to saturation with Miracle Gro once per week according to the dilution for indoor plants. Flowers were tagged on day of anthesis as 0 DPA.

2.2 Actin and microtubule labelling

Actin labelling with phalloidin was done essentially as previously described with minor modifications (Le *et al.* 2003). Briefly, individual ovules were carefully dissected from 2 DPA flowers and gently rocked in PEMT buffer containing 100 mM PIPES pH 6.9, 10 mM EGTA, 4 mM MgCl2, 0.1% triton X-100, with 2% freshly prepared paraformaldehyde and 0.5% glutaraldehyde for 1 hr, washed twice in PEMT for 10 min, then labelled with 200 nM Alexa 488 phalloidin in PEM buffer with 1 % glycerol overnight. Samples were mounted in Vectashield (Vector Laboratories Inc., Burlingame, CA) mounting media and visualized using confocal fluorescence microscopy. For microtubule labelling, the identical ovule dissection and fixation procedures were followed; however, after fixation, the freeze shattering approach was taken to fracture the cell walls and gain access to the cytoplasm for microtubule labelling exactly as described previously (Qiu *et al.* 2002).

2.3 Fibre cell morphometry and cytoskeleton quantification

2.3.1 For tip radius of curvature labelling. Ovules were harvested in the morning from 1, 3 and 6 DPA flowers that were staged based on open flower morphology at 0 DPA. Ovules were mounted in 10 mM HEPEs pH 5.0, 0.2% D-glucose and imaged using DIC microscopy. Images were acquired from fibre apices that could be clearly resolved and tip radius of curvature was measured as the radius of the circle with a perimeter shape that matched the curvature of the apical cell wall. For microtubule quantification, fibre cells were selected for analysis if they had an intact apex and uniform tubulin labelling along their length. Confocal image processes are as follows: Gaussian blur at a sigma radius of 0.7; unsharp mask image sharpening with a radius sigma of 0.7 and a mask weight of 0.6, then despeckled to remove single pixel noise. To score for the presence or absence of an MDZ and measure its size relative to fibre tip radius, fibres oriented with their long axis horizontal and image planes from one cortical surface to a medial longitudinal plane were projected. The tip radius of curvature and the perimeter distance of the MDZ were measured. Cell shape at the apex was measured after increasing image brightness to reveal weak cytosolic signal at the extreme apex. To quantify the mean angle and coherence of microtubules relative the long axis of the cell, images from 10 well-labelled cells were rotated to place the long axis of the cell horizontally and microtubule features were analysed using the OrientJ plug-in for Image J (Puspoki *et al.* 2016).

2.4 Reflected light and live cell confocal imaging

For live cell imaging *Gossypium hirsutum* cv.coker were grown in the CSIRO greenhouse space and harvested at 1 or 2 DPA. For intracellular flow analysis, ovules were dissected from flowers at 2 DPA and immobilized on glass slides using the Kwik-cast silicone epoxy (World Precision Instruments, Sarasota, Fl) and submerged in 2% glucose, 25 mM MES pH 5.7 in a ~1 mL chambered slide that was formed with a vaseline gasket and standard no. 1.5 cover glass. Ovules were immediately imaged on a Leica SP8 confocal microscope. For reflected light imaging, the notch filter was removed from the light path and a resonant scanner was used to enable fast scanning of 3 to 5 image planes per at 200–500 ms time points to improve particle tracking. To test for the actin sensitivity of cytoplasmic streaming using Latrunculin B (Sigma-Aldrich, St. Louis, MO), ovules were mounted in the standard chambered slide setup and motility was observed and imaged prior to inhibitor treatment. Then the mounting media was perfused with 100 µL of 10 µM Lat B in 0.1% DMS0 to give a final concentration of ~1 µM LatB. Control buffers lacking LatB had no noticeable effect on organelle motility. Only limited motility could be observed within 5–6 min after LatB treatment, and at later time points motility was completely eliminated. To detect acidified vacuoles, the fibres were stained with 10 µM 2′,7′-Bis-(2-Carboxyethyl)-5-(and-6) Carboxyfluorescein, Acetoxymethyl Ester (ThermoFisher) for 1 hr, rinsed 3× in imaging buffer, and then mounted for live cell imaging using the chambered slide system.

2.5 Cell wall thickness measurements

Dissected ovules at 1 DPA were fixed in 2% glutaraldehyde and 2% paraformaldehyde in microtubule stabilization buffer described above. They were then post-fixed in 1% osmium tetroxide containing 0.8% potassium ferricyanide. Additional heavy metal staining was done to improve SEM imaging (https://ncmir.ucsd.edu/sbem-protocol). Samples were incubated in filtered 1% thiocarbohydrazide for 20 min, then in 2% osmium tetroxide for 30 min and in 1% uranyl acetate overnight. The next day samples were incubated in Walton's lead aspartate at 60 °C for 30 min. After each incubation, the samples were rinsed thoroughly. Finally, samples were dehydrated with a graded series of ethanol, transferred into acetonitrile and embedded in EMbed-812

resin. Embedded samples were glued to SEM pins, trimmed and faced, grounded with silver paint, and sputter coated with platinum. Blockface sectioning and imaging was carried out using a ThermoFisher Teneo Volumescope. An ultramicrotome with diamond knife installed inside the microscope chamber was used to remove 40 nm slices incrementally. At each slice increment, the block face was imaged. Multiple images were recorded from regions of interest in the block face. Typically, regions of interest were collected at 6Kx6K pixel resolution. Several different regions and/or magnifications were collected at each slice increment. The samples were not electrically conductive; therefore, images were collected in a low-vacuum mode using a purpose designed backscatter detector. Accelerating voltage 2KV was chosen to control depth of imaging. The goal is to match imaging depth with slice increment. Because the signal is low using this imaging method, it is necessary to have beam dwell times of 3 µs. Image resolution was 8.14 nm/pixel and cell wall thickness measurements were taken as previously described (Yanagisawa *et al.* 2015).

2.6 Bead labelling and axial strain analyses

1 DPA cotton ovules were dissected from greenhouse grown *Gossypium hirsutum* and placed directly in liquid ovule culture media (BT media, Beasley and Ting, 1974) for 12 hr at 30 °C. Deep red fluorescent polystyrene beads (0.17 µm diameter, Molecular Probes) were applied to the chalazal end of the ovule followed by several washes using fresh BT media. Ovule was placed in a silicon chamber system with BT media and held in place by adding Vaseline to the chamber end and embedding the micropyle end to it for stability. Images were collected using a 50x LU-Apo 0.55 numerical aperture (N.A.) long working distance objective and a Coolsnap HQ camera (Photometrics) mounted on a Nikon 80i microscope. Image stacks were collected at 3–5 hour intervals using a z-step of 0.5µm. Images were collected sequentially using brightfield to capture fibre shape and bead fluorescence through 561 bandpass filter for bead signal. Device was controlled using Slidebook software version 6.0.15 (Intelligent Imaging Innovations, Denver, CO). Fibres with stable beads with good coverage were identified and rotated vertically such that the fibre tip pointed up. Line ROIs across the lowest bead were used to align all the time-points. Bead tracking was performed using MTrackJ plugin using a 25 × 25 µm pixel region and the bright centroid the computer assisted local snapping feature. The distance between bead pairs along the longitudinal cell axis was measured as a function of time and a linear fit equation was obtained to calculate the total displacement. If the total displacement was below the image resolution, then a growth rate of zero was assigned to the pair. The percent normalized axial elongation rate was obtained using the following formula:

$$\%\ NAER = \frac{Distance_{initial} - Distance_{final}}{Distance_{initial}} * Hours^{-1} * 100$$

2.7 3D finite element model of tapering fibres

A finite element (FE) model of cotton fibre growth was created using the commercial finite element software Abaqus 2019. The cotton fibre was modelled as a composite shell in which the diameter at the flank edge was constant. This constraint defined the radius of 8 µm and served as a boundary condition at the fibre base. The FE model was discretized using 3- or 4-node shell elements (S3R or S4R) with the maximum size of 100 nm to minimize the effect of mesh size on the result and have convergence with the implicit solver. Determination of cell wall thickness of the cotton fibres was performed by electron microscopy from STEM or TEM images in 1-2 DPA samples. This thickness was measured by averaging the thickness values from positions that did not include trapped air. For each fibre, the average thickness was based on about 10 lines that each corresponded with the distance from the outer layer (pixel) of the membrane to the cell wall outer layer. The cell wall thickness at each stage (DPA) was the average from three fibres giving a value of ~150 nm. The cell wall was modelled as an orthotropic laminate composite shell with a single dominant orientation of cellulose microfibrils (CMFs) which at the initial stages was transverse to the growth axis of the cotton fibre. The homogenized shell was constructed from two layers of a composite lamina on either side of an isotropic, viscoelastic layer. The transverse orientation of the CMFs was determined from MT array organization, from immunolocalization data in this study. A layer of viscoelastic matrix, representative of the soft material of the wall such as pectin, defined the time-dependent behaviour of the cell wall using values based on pavement cell viscoelastic properties (Hayot *et al.* 2012; Forouzesh *et al.* 2013). As with our previous trichome model (Yanagisawa *et al.* 2015), a standard linear solid viscoelastic material was assumed for the viscoelastic behaviour. The standard linear solid model includes one Maxwell element (spring and dashpot) in parallel with an additional spring. In this case, the matrix modulus has a time dependence of the form $E_{matrix}(t) = E_{inf}\left(1 + h_1 e^{-t/\tau_1}\right)$ with relaxation time τ_1 = 6.88 s, dimensionless relaxation ratio h_1 = 0.143, and matrix long-term modulus E_{inf} = 87.5 MPa. The matrix modulus and the modulus of the orthotropic lamina perpendicular to the CMFs (E_2) were assumed as 100 MPa (Zsivanovits *et al.* 2004) while the modulus of the orthotropic lamina parallel to the fibres (E_1) was assumed as 70 GPa (Santiago Cintrón, Johnson and French 2011; Mariano, El Kissi and Dufresne 2014). A Poisson's ratio (ν_{12}) of 0.45 and a shear modulus (G_{12}, G_{23}, G_{13}) of 45 MPa in all directions were assumed. The wall matrix was assumed to constitute ~85% of the cell wall with a density of 1000 kg/m^3 (Guimarães, Coelho Júnior and Garcia Rojas 2009), and the remaining volume was given material properties that were intended to mirror cellulose fibres within the cell wall, with a density of 1650 kg/m^3. For the gradual transition from the anisotropic shoulder to the isotropic zone, the isotropic zone was divided into several regions using horizontal planes. Orthotropic materials with a decreasing degree of anisotropy (higher matrix elasticity and lower fibre Young's modulus) than the shoulder were assigned. The cotton fibre was modelled as a shell reservoir under constant hydrostatic turgor pressure with a pressure on the outer wall to represent atmospheric pressure (0.1 MPa). The turgor pressure in the model was increased linearly from 0 to 0.5 MPa. The fibre growth model was constructed based on the initial length of the cotton fibres at 1 DPA (50 µm) and associated radius of curvature at the tip and definition of isotropic zone (IZ) according to the MDZ perimeter from experimental data (see Table 1 for details). The model IZ perimeter was adjusted so that the deformed model would match the tip radius of curvature (ROC) based on the microtubule depleted zone (MDZ) perimeter at different stages of growth. The growth model was written as a python script that

Table 1. Mechanical properties estimated and assigned to the cell wall in the FE model of cotton fibre growth. Properties of the composite material include the density of the fibres and matrix, the Young's moduli, E_i, the shear moduli, G_{ij}, Poisson's ration ν_{12}, volume percentage V, thickness and the initial cellulose microfibril angle.

Type of Structure	Material	Density (kg/m^3	E_1 (MPa)	E_2 (MPa)	ν_{12}	G_{12}, G_{23}, G_{13}(MPa)	V%	Thickness (nm)	CMF angle (°)
Composite	Orthotropic shell (fibre)	1650	70000	100	0.45	45	15	22.5	0
Laminate	Viscoelastic (matrix)	1000	100	–	0.45	–	85	127.5	–
Isotropic	viscoelastic (MDZ)	1090	400	–	0.45	–	100	150	–

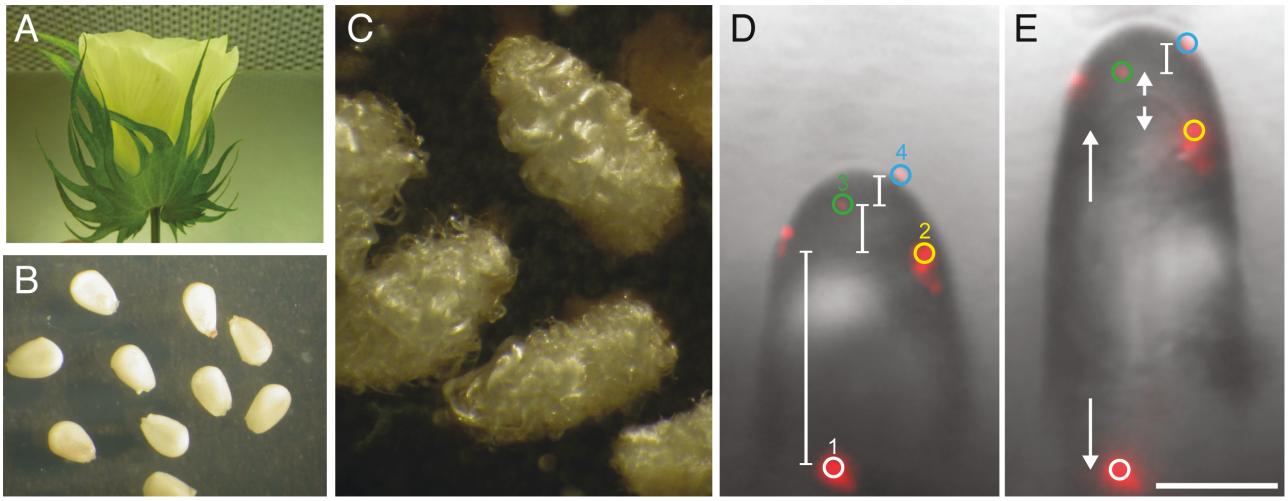

Figure 1. Early stage fibres employ a diffuse growth mechanism. (A) Cotton flower at 0 DPA. (B) Dissected ovules from a 0 DPA flower, the wider chalazal end of the ovule is the first to initiate fibres and all imaging and localization analyses focused on this subregion. (C) In vitro cultured cotton ovules. (D) High magnification bright-field image of a developing fibre at 1.5 DPA labelled with fluorescent particles. (E) Same cell as in (D) at 2 DPA with the trackable particles circled, numbered and coloured. The initial axial distance between bead pairs is indicated with blocked lines in (D) and equivalent length arrows in (E) in instances where growth was detected. Fibre images were aligned relative to bead 1. Bar = 10 μm.

interfaced with Abaqus. The location of the publicly available model is provided in the Model and Data Availability section.

3. RESULTS

3.1 Cell diameter is defined early in fibre development

At 0 DPA, the flower opens fully, and the ovules have a very smooth appearance (Fig. 1A and B). This developmental program can be reconstituted in vitro, as cultured ovules can generate highly elongated fibre cells that resemble in situ fibre both in their developmental timing and changes in cell wall composition (Meinert and Delmer 1977; Triplett 2000). We wanted to test directly for diffuse growth by labelling early stage in vitro grown fibres with fluorescent particles on the cell wall. Time lapse imaging of cotton fibres has never been achieved, and was complicated further by our microscopy setup operating at 22 °C, far below their optimal growing temperature. Nonetheless, we were able to obtain one useful time series in which the fibre clearly elongated and 4 trackable particles adhered to the wall for 4 observations within the total interval of 11 hr (Fig. 1D and E; Supplementary Information—Movie S1). As expected, this early growth phase included a diffuse growth component. The axial distance between particles 1 and 2 increased by 10.2 μm over the 11-hr interval which corresponded to a normalized axial elongation rate of 5.3% per hour. Bead pairs 2 and 3 had a detectable axial distance increase of 0.8 μm and this corresponded to a normalized axial elongation rate of 1.7% per hour. No significant growth was detected between beads 3 and 4 because of their close proximity. These axial strain data indicate that cell elongation occurs broadly on the cell surface and may be faster in more basal domains. These data are consistent with prior observations supporting a clear role for polarized diffuse growth during fibre elongation (Ryser 1977; Seagull 1990; Tiwari and Wilkins 1995; Graham and Haigler 2021). Our data and ultrastructural data of early stage fibre apices (Tiwari and Wilkins 1995) are not consistent with a tip growth component to fibre elongation. However, based on our limited analysis of subcellular strain in only one fibre cell with sparsely distributed fiducial marks, we cannot rule out a tip growth component to the early phase of fibre elongation.

We next wanted to determine the precise developmental timeline of fibre tapering of *G. hirsutum*, which is the most widely cultivated form of cotton, and *G. barbadense* (commonly known as pima), which is lower yielding compared to *G. hirsutum* but has longer and thinner fibres that yield a higher thread count, a softer feel, and increased commercial value. Variability among genotypes in fibre tapering was first reported by Butterworth (Butterworth *et al.* 2009). More recently tapering has been shown to be nearly complete by 2 or 3 DPA (Stiff and Haigler 2016). In our growth conditions, 1 DPA fibres of both *G. hirsutum* and *G. barbadense* had a mean tip radius of curvature of ~7.5 microns (Fig. 2A, E, and I); however, the distributions were significantly different between *G. hirsutum* and *G. Barbadense.* As previously shown (Graham and Haigler 2021), the differences are driven largely by the higher variability in *G. hirsutum* diameter. Both genotypes displayed a reduced cell diameter in nearly all cells at 2–6 DPA compared to 1 DPA (Fig. 2I); however, the increased variability in *G. hirsutum* diameter compared to *G. barbadense* and significant differences between genotypes persisted at each of the subsequent stages examined (Fig. 2I). The variability in tip radius in *G. hirsutum* has been reported previously (Stiff and Haigler 2016; Graham and Haigler 2021). These results indicated that tapering occurs in most fibres in both genotypes, but *G. hirsutum* has a more variable tip radius at each time point examined. Variable tapering in *G. hirsutum* has been proposed to reflect two distinct fibre types (Stiff and Haigler 2016; Graham and Haigler 2021), but could also be explained by inconsistent tapering in the population.

3.2 Actin localization and intracellular flow patterns in tapering fibre cells

Both the actin and microtubule cytoskeletons cooperate to mediate tapering in aerial trichoblasts (Yu *et al.* 2019). We first analysed actin-based functions in tapering *G. hirsutum* fibre cells. *Gossypium hirsutum* was used for all subsequent imaging experiments because its fibres had far less background fluorescence compared to *G. barbadense* In tapering Arabidopsis leaf hairs, a highly organized longitudinal actin bundle network mediates patterned long-distance intracellular transport (Yanagisawa *et al.* 2015). An apical patch of activated actin-related protein (ARP) 2/3 complex generates a localized actin meshwork that positions longitudinal bundles and dictates cellular scale flow patterns. These activities are required to modulate cell wall thickness during trichoblast expansion (Yanagisawa *et al.* 2015). In leaf hairs, the apical actin patch is easily observed in whole-mounted cells using antibodies or phalloidin (Le *et al.* 2003; Basu *et al.* 2004), but is not detectable using live cell probes based on the actin binding domains ABD or Lifeact (Dyachok *et al.* 2008; Yanagisawa *et al.* 2015). In young cotton fibres, an ABD2-based GFP reporter was used to visualize actin bundles (Yu *et al.* 2019). The authors reported that they did not detect any isolated actin cap structures but did describe an actin network in which longitudinal 'actin cables traversed the shank and linked to fine F-actin structures at the tip'. If cotton fibres controlled the actin network in a manner similar to Arabidopsis leaf hairs, this type of organization would be expected.

To analyse actin networks in tapering cells, 1 and 2 DPA whole mounted ovules were fixed and stained using Alexa Fluor 488 phalloidin as described previously (Le *et al.* 2003). The labelling was simple and effective since the ovule contained thousands of similarly staged cells. Among those that were close to the cover slip, we could easily select fibres that had uniform actin labelling. Fibres with different degrees of tapering had longitudinally aligned actin bundles in the shank, many of which were subcortical (Supplementary Information—Fig. S1). These data indicate that long-distance roadways for intracellular transport are not restricted to the cell cortex by a large central vacuole.

The tip organization of actin was examined closely in a population of tapering fibres. There was not a single example of an apically concentrated actin meshwork along the collar or at the apex that is commonly referred to as 'fine' actin. Instead, we noted two distinct apical organizations. Of the 45 fibre cells examined, 28 had actin bundles that entered the extreme apex and looped around the tip following the contour of the cell shape (Fig. 3A–C). Fourteen of 45 fibres had a distinct organization in which a population of aligned bundles terminated at a similar location distal to the extreme fibre apex (Fig. 3D and E). The apex was not completely free of actin, but the thick bundles clearly did not traverse the apex. Three cells had an intermediate appearance and did not clearly fit into either of the above categories. These results suggest that the actin network oscillates between two distinct organizations during the tapering process.

In Arabidopsis leaf hairs, individual bundles mediate efficient linear transport of secretory organelles that is biased toward the tip or base (Szymanski *et al.* 1999). Because plant myosin is +-end directed motors, actin filaments probably have a parallel organization within the bundles. Intracellular particle flow analysis provides a useful assay for the actin-based transport. This is very challenging in cotton fibres because the movement is several microns/sec and the tracks meander longitudinally in a large cytoplasmic volume and most particles exit the image plane after a few frames. Here a new live cell imaging workflow was developed to better analyse the patterns of intracellular transport. Subsets of plant organelles have an interesting property of reflecting incident laser light in point-scanning confocal systems (Fig. 4). This is likely due to a difference in refractive index between the cytosol and the lumen of an organelle that is densely packed with secretory cargo. Some degree of specificity of the reflected light signal in a fibre apex is shown in Supplementary Information—Fig. S2. The transmitted light image detects a dense population of organelles that also are detected using reflected light imaging (Supplementary Information—Fig. S2A and B). Acidified vacuoles of different sizes are labeled with the vital dye BCECF, but these are not the particles that have a reflected light signal (Supplementary Information—Fig. S2C).

The reflected light signal can originate from the surface of the fibre apex, but unlike the intracellular dense particles, the cell surface reflection signal does not move (Fig. 4A–C). The bidirectional movement of the dense particles along longitudinal tracks was completely dependent on an intact actin cytoskeleton, since the motility is rapidly blocked by 1 μM latrunculin B (LatB), which specifically targets the actin cytoskeleton (Supplementary Information—Movies S2 and S3).

Rapid 5D live-cell imaging was used to capture the movement of numerous particles in a trafficking lane that were often in the range of 3-5 μm/sec. An example of the fibre analysed using transmitted and reflected light is shown in Fig. 4A. In the subregions indicated 4 image planes in each channel were acquired in 50 ms and converted to maximum projections at each time point. A time lapse of the reflected

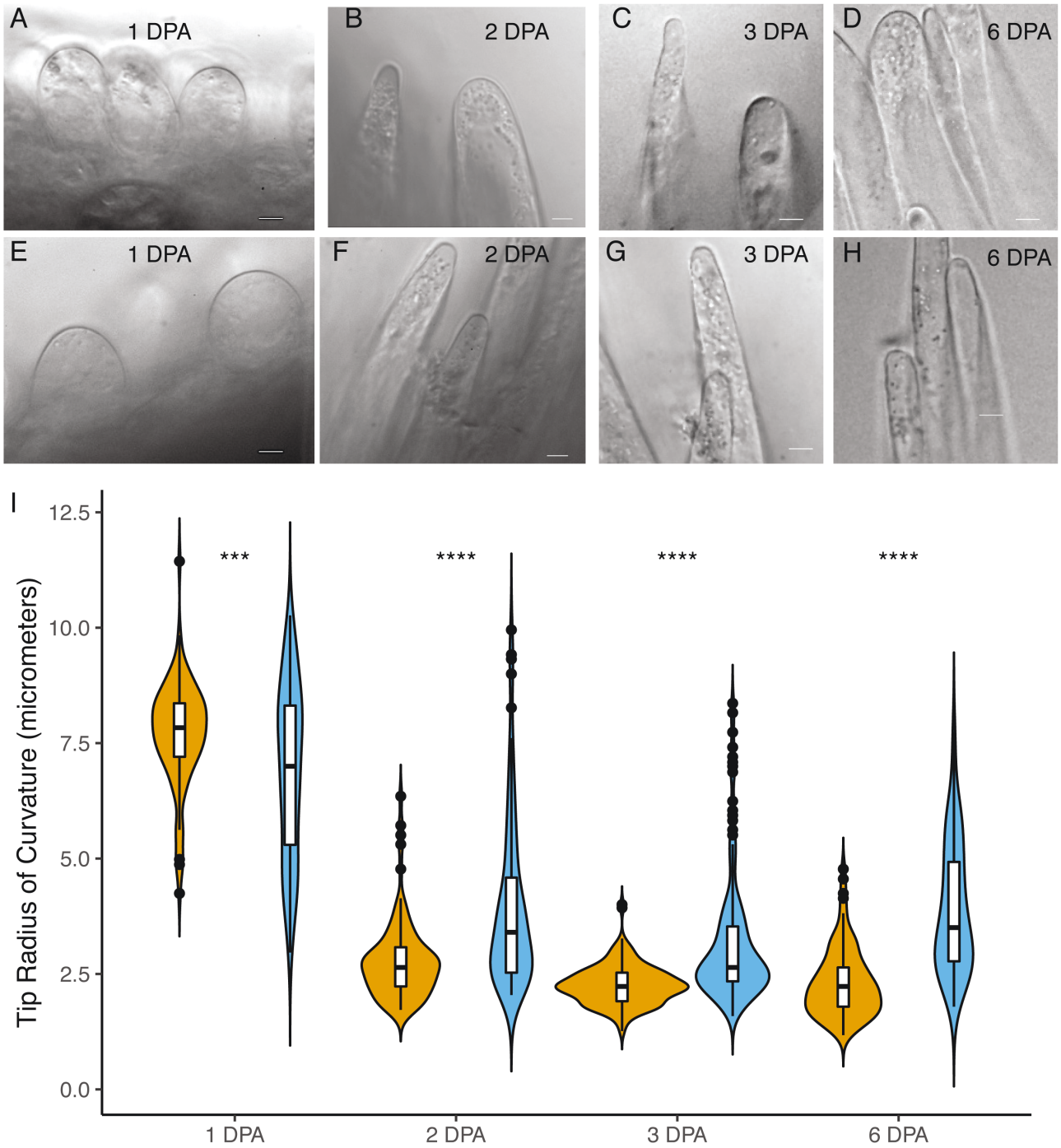

Figure 2. Timing and extent of fibre tapering at early stages of fibre development. (A–D) Developing fibres on the chalazal end of *G. hirsutum* ovules at the indicated time points. (E–H) Developing fibres on the chalazal end of *G. hirsutum* ovules at the indicated time points. (I) Violin plots of distributions of fibre radius of curvature at the apex at the indicated stages, mustard, *G. barbadense*; aqua, *G. hirsutum* Bars = 2 µm.

light channel is provided in Supplementary Information—Movie S3. A single point overlay of the reflected and transmitted light signals is shown in Fig. 4F, indicating that the objects generating reflected light signal are indeed organelles that can be seen in the transmitted light channel. A summed projection of the reflected light channel is shown in Fig. 4G and H indicating that the particles move along linear tracks, which must be actin bundles based on the latrunculin B results. Many of the particles entered the imaging volume from the tip and followed

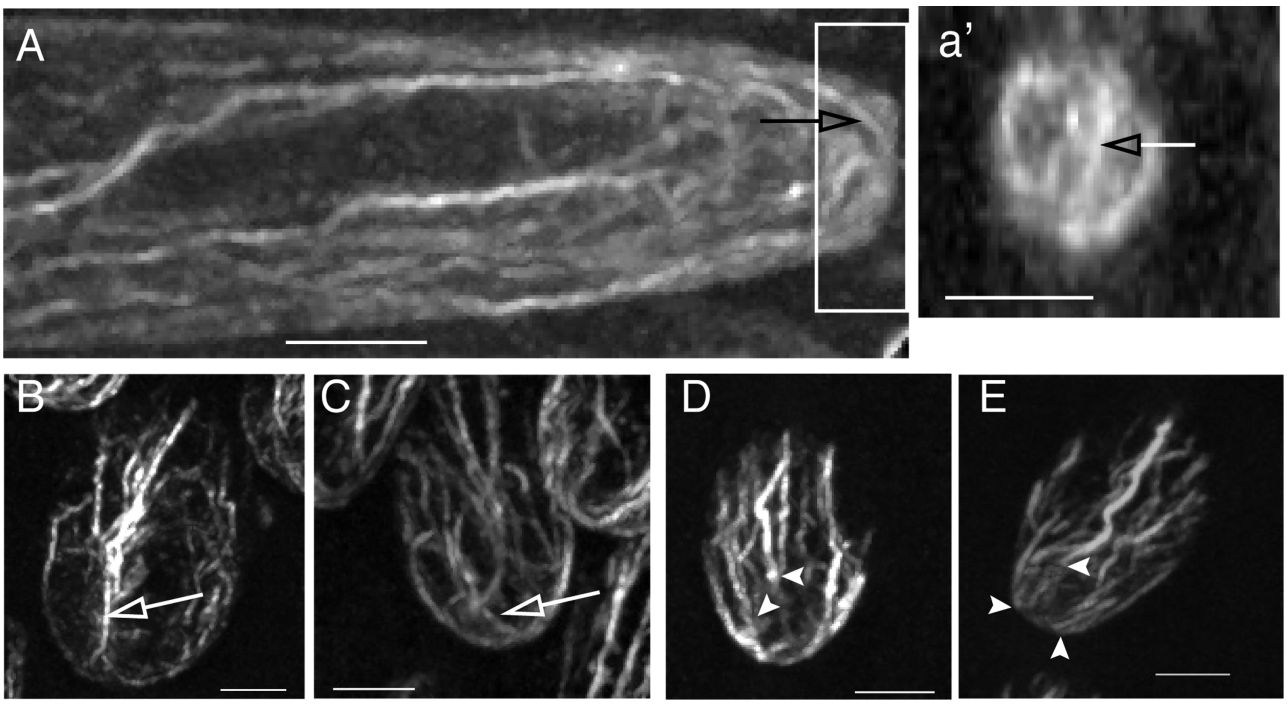

Figure 3. Organization of the actin cytoskeleton in whole-mounted cells labelled with fluorescent phalloidin. (A) Projected image of the side view of a tapering fibre with a longitudinally aligned actin bundle network. White box, region of image stack that was resliced in the y/z plane and projected in a'. (B–E) Projections of oblique face on views of actin bundles in fibre apices. The apical dome is evident in each panel. (B and C) Example apical localization of actin bundles that follow the arced contour of cell apex. (D and E) Example apical organization in which most actin bundles and filaments terminate at the cortex just proximal to the fibre apex. Arrows mark actin bundles that extend along the cortex and transit the apical dome. Arrowheads mark actin bundles that terminate near the branch apex. Bars = 2 μm.

curved trajectories at that reflected cell geometry at the apex (Fig. 4G). This pattern would be explained by the presence of actin bundles that curve around the fibre tip. Another example 5D time lapse revealed a dense population of organelles that followed curved trajectories that mirrored the shape of the fibre apex (Supplementary Information—Movie S4). These analyses demonstrate that the curved bundles at the apex are functional tracks that don't necessarily involve tip-directed transport. It seems likely that the fibre tips might switch between two different actin configurations, and two channel imaging of actin and organelles will be needed test for distinct flow patterns. Taken together, these time-lapsed and actin localization experiments demonstrated the functional transport properties of the actomyosin system along the shank and around the apex of tapering fibres.

3.3 Microtubule localization in tapering fibres

Since cotton fibres appear to employ the microtubule-CESA system to pattern tapering, this cell type provides another opportunity to quantitatively analyse the degree to which microtubules are ordered and their occupancy of the fibre apex. By extrapolating these microtubule patterns to those of expected arrangement of the cellulose fibres, it is possible to generate FE simulations with fibre-reinforced walls to predict tapering mechanisms, as done for leaf trichoblasts (Yanagisawa *et al.* 2015). At present, quantitative information on cortical microtubule localization and degree of ordering in tapering fibre cells is limited. Microtubule organization in 1 DPA fibres was first described as random or axial in early EM studies (Seagull 1992; Tiwari and Wilkins 1995). In a more thorough immunolocalization study of tapering fibres at 0 to 2 DPA (Graham et al., Graham and Haigler 2021) reported the presence of an apical MDZ with dimensions that were positively correlated with tip geometry, but was judged as a weaker correlation compared to that which was reported for the MDZ in tapering Arabidopsis leaf hairs (Yanagisawa *et al.* 2015). Differences could be expected because the leaf hair data came from live cell imaging using a well-established microtubule binding domain fusion (Marc *et al.* 1998; Yanagisawa *et al.* 2015). Similar lines are not available in cotton. A transgenic line expressing the EB1 fused to GFP has been used to visualize microtubule +-ends in young fibres (Yu *et al.* 2019), but the EB1 tracks from time lapsed imaging were very short and could not be used to visualize or quantify cellular-scale organization.

Here we immunolabelled tubulin in fixed whole-mounted 1 DPA fibres with a variety of diameters using the well-established freeze shattering approach (Wasteneys *et al.* 1997; Qiu *et al.* 2002 Justus *et al.* 2004; Zhang *et al.* 2013). Ovule samples processed in this manner can be efficiently screened for cells with well-placed cracks that preserve cell shape and display a uniformly labelled cytoskeleton (Fig. 5). All elongated 1 DPA fibres identified in this manner had an apical MDZ

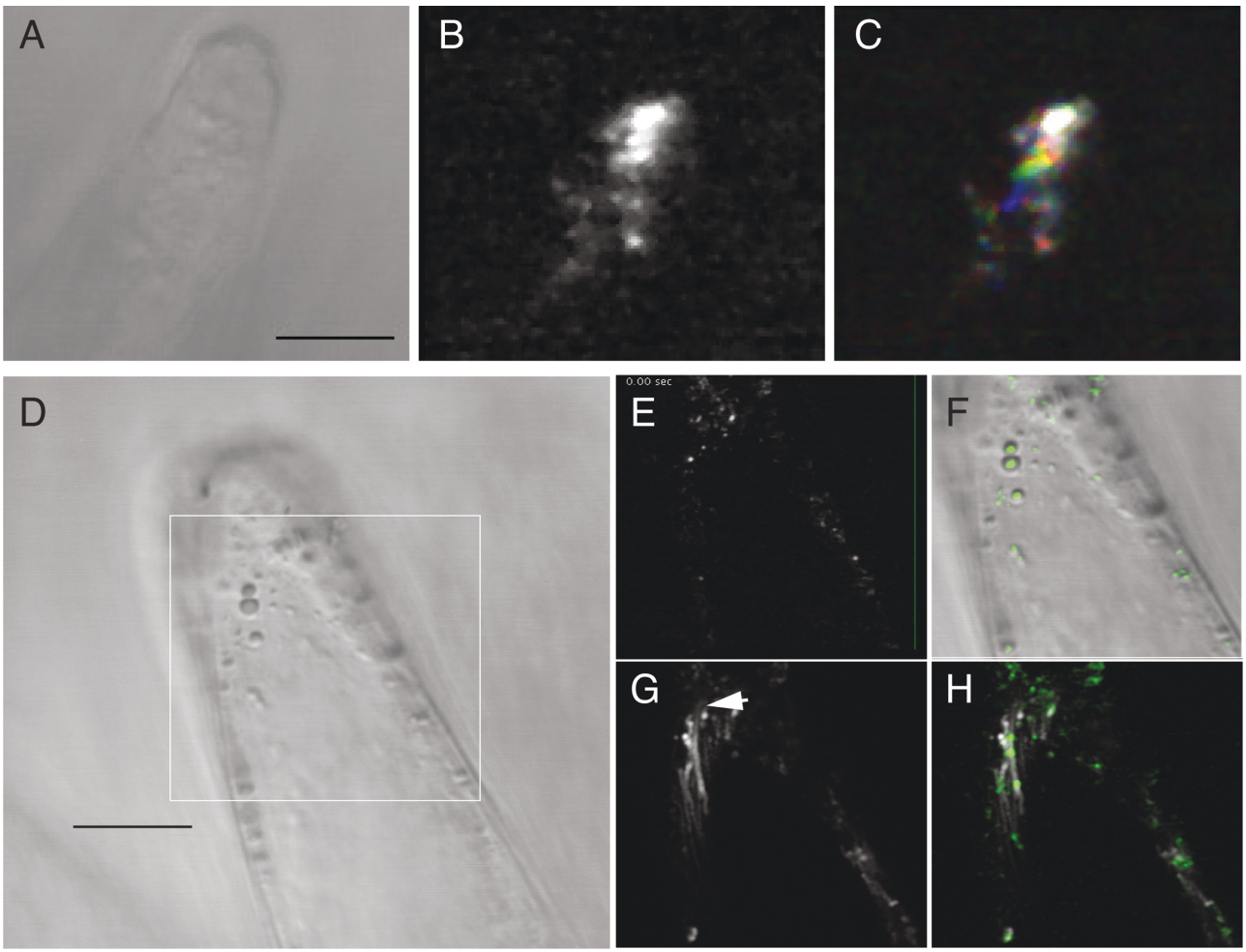

Figure 4. Long-distance flow analysis of organelles in developing fibres using 2-channel reflected and transmitted light microscopy. (A) Single plane transmitted light image of a living 1 DPA fibre. (B) Reflected light signal from the same image plane. (C) Time series image with the three consecutive time points false-coloured red, green, and blue. Non-moving objects appear white, moving objects are coloured. (D) Transmitted light image of a living 1 DPA fibre. (E) Projection of 4 image planes at a single time-point. (F) Projection of a merged imaged of the reflected light (green) and transmitted light signals (grayscale) from a single time point. (G) Summed image of the reflected light signal over a time course. (H) Summed image of the reflected light signal over a time course the organelle signal from a single time point indicating resolved particles. Arrow in (G) labels the fibre apex. (F) Bars = 5 μm.

and cortical microtubules with a net transverse alignment along the fibre shafts. Importantly microtubules were not always completely absent from the apex as revealed in a face on view (Fig. 5), but in this zone they had no clear radial alignment. Since microtubule-programmed cellulose fibre anisotropy in the cell wall is the mechanism by which microtubules affect cell shape change, this pattern is consistent with a highly anisotropic cell wall along the shaft and an isotropic domain with randomly aligned fibres at the apex.

To analyse microtubule order more quantitatively as a function of cellular locale, the geometry of the MDZ and degree of microtubule alignment were measured in a population of tapering fibres with a range of cell diameters. Eleven cells were uniformly labelled with a well-preserved apex, and all displayed a clear MDZ (Fig. 6; Supplementary Information—Fig. S3). The microtubule-depleted cytoplasm near the apex could be visualized by altering the brightness and contrast to track the cell boundary (Fig. 6). Fibre cells at early (Fig. 6A and B), middle (Fig. 6C and D) and late (Fig. 6E and F) stages of tapering all had an apical MDZ. The geometry of the MDZ and the tip radius of curvature were correlated (Fig. 8A). The mean microtubule angle and the coherency of the network of each cell were quantified using the OrientationJ plugin in Image J. There was variability among and within cells in terms of the microtubule orientations; however, the mean angle along the fibre shafts was 92° ±8° (N = 11) relative to the long axis of the cell.

3.4 A plausible mechanism for fibre tapering based on FE modelling

The microtubule and actin localization data shown above indicate that the two cytoskeletal systems function in a complementary manner to

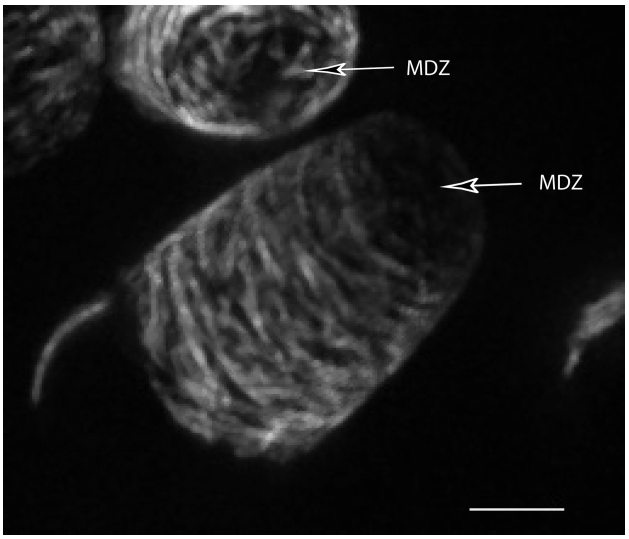

Figure 5. Immunolocalization of microtubules in whole mounted *G. hirsutum* fibres at 1 DPA. Fibres were fixed, frozen in liquid nitrogen, and the cell wall was cracked to allow antibody access using the freeze shattering method. The apical microtubule depletion zone (MDZ) is labelled for two different fibres, the upper one contains a fortuitous face-on view the reveals the presence of some randomly oriented microtubules in the apex. MDZ of both cells labelled with arrows, bar = 5 μm.

pattern the cell wall and create a tapered growth pattern. The microtubule data were combined with other experimental data to create a full 3D FE model (see Methods for details) of early-stage fibres and evaluate the plausibility of microfibril-based anisotropy in the shafts and the MDZ to control tapering and polarized fibre elongation, respectively. The model uses realistic values of turgor pressure, includes viscoelastic material behavior, and is based on a fibre-matrix composite that resists radial cell expansion. Growth is simulated using a multi-step growth process that maintains the wall composition history. The fibre growth model was initiated based on geometry and cell wall thickness of fibres at 1 DPA (Fig. 7A). The relationship between the tip radius of curvature (ROC) and the measured MDZ was defined using a linear fit to the data shown in Fig. 8A. An isotropic zone (IZ) was used as a control parameter in the model and the IZ reflected the prediction of randomly oriented CMFs in the MDZ which would have no organized microtubules to provide patterning information. The associated ROC at the tip after the model had deformed was matched iteratively to experimental data (see Table 1 and Fig. 7B for details). In the iterative growth model, the IZ region was defined with isotropic properties while the wall outside of the IZ was defined as orthotropic with CMF alignment transverse to the medial longitudinal axis of the cell. The first cycle began with an IZ perimeter length of 7.7 μm based on the most blunt cell data in Fig. 8A. Next, a pressurization step deformed the model and the wall was allowed to relax fully (i.e., due to the viscoelastic effect) which resulted in the final geometry for this step. Then, the resulting ROC was compared with the measurement profile of ROC (Fig. 2I) to see if it fell within bounds of the experimental data. If so, the next cycle was initiated with the new IZ based on the deformed shape from the previous cycle. Otherwise, the IZ perimeter was either increased or decreased according to the deviation in the ROC from the allowable range and the previous cycle was repeated with a new IZ perimeter (Fig. 8B and C). The bounds of the ROC as a function of fibre length were defined using a spline fit to the measurement data (Fig. 2I; result shown in Fig. 8C) based on published length data in terms of DPA (Graham and Haigler 2021). This process was used sequentially to generate a tapering and elongating cotton fibre. Figure 8C shows the values of IZ perimeter with ROC for the computations. The green circles are results for ROC from the iteration process that fell within the acceptable range while the yellow triangles are those that were led to cell shapes that were out of the acceptable range of ROC (Fig. 8C). In general, the MDZ and inferred IZ perimeter values and the resulting ROCs followed the linear trend in the experimental data (Fig. 8A). However, in the fibre tapering simulations, convergence at each step became more difficult as the ROC approached the plateau defined when the fibre was ~300 μm long and the ROC was ~2.5 μm (Fig. 8B). At this point, the downward trend in IZ perimeter length would not allow the model to progress to the next step. Here, a slight increase in the IZ perimeter was needed to allow the computations to continue forward (Fig. 8B). These results show that the model can accurately predict the constant tip ROC for later stages of growth under the condition that the IZ plateaus to a constant value. Finally, the fibre length from the model was compared with experimental data (Graham and Haigler 2021) covering 1-4 DPA as shown in Fig. 8D with excellent agreement. For this comparison, the 4 DPA fibre was assumed to have a length of 800 μm. The overall tapering process from the model is shown in Fig. 8E as the fibre extends from 50 to 300 μm.

The model was also used to generate spatial maps of the magnitudes and directions of stress and strain (Fig. 9A and B). Geometry and material properties had major influences on both parameters. It was likely that the predicted stress concentration at the base of the apical dome was an artefact of the model due to the abrupt change from material symmetry (anisotropic to isotropic) at the transition out of the apical dome (Fig. 9A). A more gradual transition based on a material gradient that was smoothed across 5 elements spanning ~500 nm of cell surface (see model details) made this stress pattern smoother (Fig. 9A). The model with smooth transitions indicated that both the magnitude of wall stress and the degree of alignment increased away from the apical dome. This was expected based on the cylindrical geometry of the cell. The magnitudes of stress and strain were spatially correlated as expected (Fig. 9A) and their directions in the fibre shaft were orthogonal (Fig. 9B). The circumferential alignment of the CMFs restricted parallel expansion but allows longitudinal extension, as expected based on direct observations of microfibrils in native cell walls (Zhang *et al.* 2021). Since both wall stress patterns (Hamant *et al.* 2019) and cell geometry (Ambrose *et al.* 2011) can influence microtubule ordering and stability, the model was used to analyse how these parameters interacted during simulated growth. The changes in maximum principal stress with respect to subcellular position, computational step and ROC reduction are shown in Fig. 9C. The stress near the bottom of the shaft was nearly constant as expected because of the constant turgor pressure and geometry. Near the top of the shaft and shoulder regions, the stress was reduced at similar rates with step due to the pronounced effects of reductions in fibre diameter in these regions

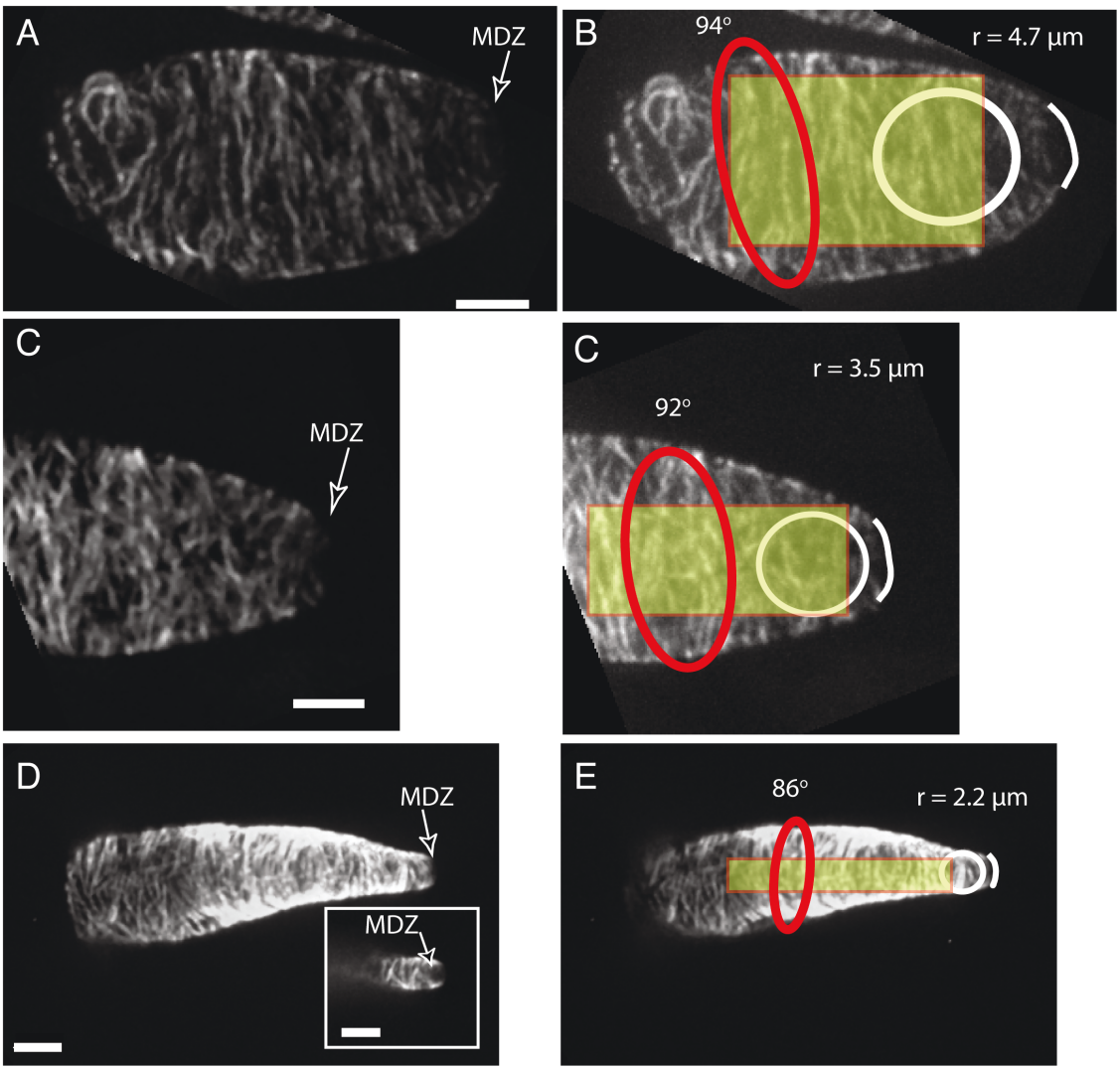

Figure 6. Analysis of the MDZ and microtubule orientation as a function of fibre tapering. Example images at the early (A and B), mid (C and D), and late (E and F) stages of tapering. Microtubule localization along the fibre shaft and the location of the MDZ are shown in the left panels. Quantification of mean microtubule angle and coherency along the fibre shaft and tip radius of curvature are labelled in the right panels. Hand drawn arc at the cell apex indicates the location of cell apex that was marked on raw images that were adjusted high brightness and contrast adjusted. Bars = 5 µm.

(see also Fig. 8E). Stress values at isotropic apex were nearly constant through the first 20 cycle during which tapering was nearly complete and fell gradually throughout the remainder of the simulation. These results indicate that the dynamic range of stress from apex to distal shaft domains remains rather constant during growth, but the steep spatial gradient of stress in the apical regions is dampened as tapering progresses. Potential mechanisms by which stress gradients and cell geometry might influence the microtubule array are discussed below.

The FE model also showed the impact of CMF orientation on the deformation of the fibre during the growth cycles (Fig. 10). CMF orientation angles that deviated from 90° (assuming constant wall properties) resulted in an unrealistic swelling of the fibre (Fig. 10A and B). Orientations near 90° showed extension without fibre swelling but radial expansion increased if the CMFs were aligned more closely with the longitudinal direction. This result is consistent with the tight thresholds for anisotropic expansion of leaf trichoblasts in Arabidopsis (Yanagisawa *et al.* 2015) and highlights the importance of CMF orientation angle during anisotropic expansion. The FE model was also used to examine the impact of spatial variations of the CMF orientation (Fig. 10C and D). The model predicted apical swelling when the IZ extended beyond the apex of the hemispherical dome (Fig. 10C). Randomly oriented CMFs within the shaft (Fig. 10D) did not provide sufficient stiffness such that bulging occurred. These aberrant shapes were similar to those observed by Wilkins (Tiwari and Wilkins 1995) in 1-2 DPA that were treated with microtubule depolymerizing drugs. These simulations indicate

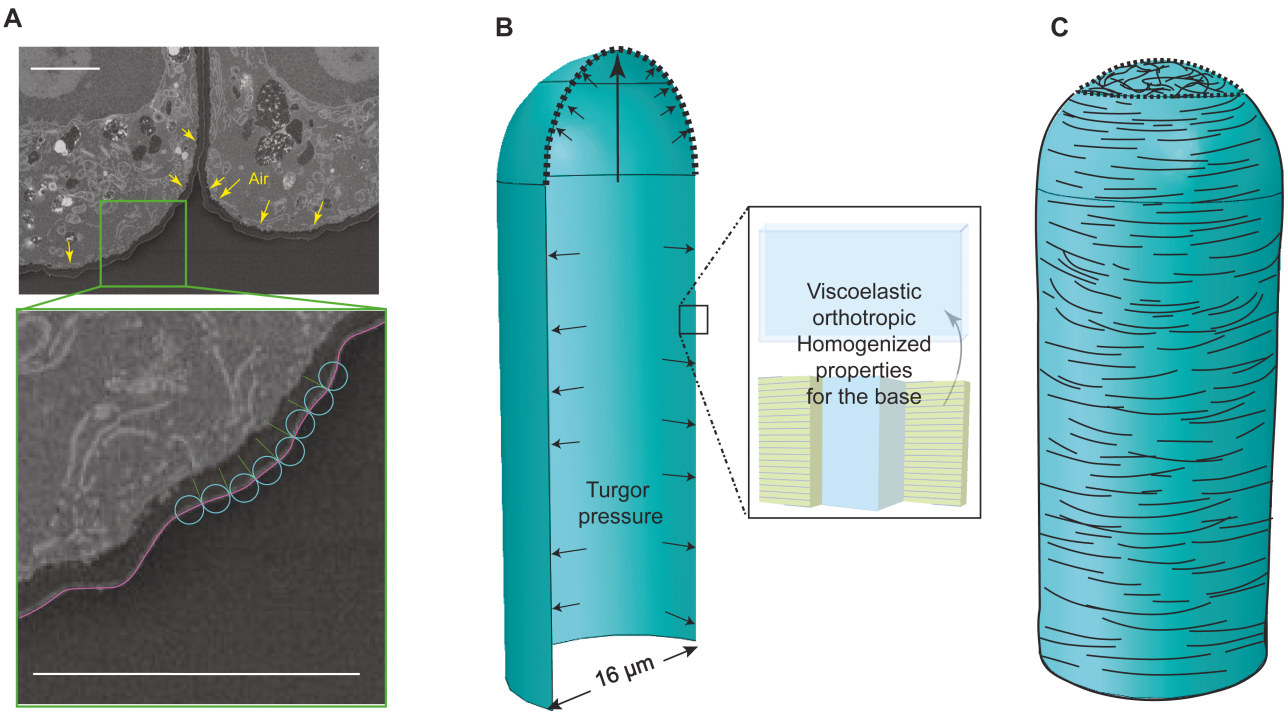

Figure 7. Cell wall geometry and basic description of the finite element (FE) model of the cotton fibre: (A) Cell wall thickness measurements from a 1 DPA fibre imaged using transmission electron microscopy. Measurements were taken from regions that did not have air space (the darker areas denoted by the yellow arrows in the image); scale bar = 1 μm. (B) Initial geometry and material organization the FE model. A viscoelastic, orthotropic composite shell is used to represent cellulose microfibrils embedded within a soft matrix. The isotropic zone (IZ) perimeter is denoted with dashed line and the arrow shows the radius of curvature (ROC). (C) Random fibres present at the tip in the IZ are modeled by using isotropic behaviour while the shaft is modelled as a composite shell based on two layers of an orthotropic shell (laminae) surrounding an isotropic viscoelastic layer. The plane defining the transition from anisotropic to isotropic wall properties is marked by the dashed square.

that the cell must maintain a strongly transverse cortical microtubule array during the entire elongation phase in order to preserve a constant cell diameter along its length.

4. DISCUSSION

A major challenge in plant morphology research is to gain mechanistic understanding of the most relevant interactions between biomechanical processes and their underlying cytoskeletal control. The combined use of FE modelling with multivariate live cell imaging is revealing how gradients of morphogens and mechanical signals interact to dictate local growth patterns (Chickarmane *et al.* 2010; Fox *et al.* 2018; Kierzkowski *et al.* 2019; Belteton *et al.* 2021). However, anisotropic growth is often an assigned parameter in growth models and the means by which individual cells polarize is poorly understood. In some ways quantitative analyses of growth are simplified by the fact that the process is irreversible, the geometric features are rather large and easily resolved using light microscopy (Szymanski and Cosgrove 2009). High-resolution FE modelling is useful in a single cell context because it can be used to predict the subcellular material properties that are most important for the observed growth and the cytoskeletal basis of their patterning (Yanagisawa *et al.* 2015; Belteton *et al.* 2021). Trichoblasts are an excellent model for such studies, and in tapering Arabidopsis leaf hairs, anisotropic growth is driven by a combination of a cell wall thickness gradient, a strict threshold requirement for aligned fibres in the cell shaft, and a constricting isotropic tip zone (Yanagisawa *et al.* 2015). In this paper, a multiparametric experimental analysis and a realistic 3D FE model were used to uncover conserved morphology control mechanisms of cotton fibres.

4.1 Cytoskeletal and cell wall systems that enable polarized fibre elongation

Our results indicate that fibre expansion and tapering occur via an anisotropic diffuse growth mechanism that involves tight spatio-temporal control of wall properties at the apex, shoulder and shaft. Superficially, fibre elongation, like that of leaf trichoblasts, resembles tip growth and a mixed mode of growth that involves global anisotropy control through the microtubule-microfibril system and tip growth modulation through the actin system are frequently invoked (Kim and Triplett 2001a; Pang *et al.* 2010; Qin and Zhu 2011; Haigler *et al.* 2012; Stiff and Haigler 2016; Graham and Haigler 2021). The existing experimental support for a microtubule-patterned diffuse growth mechanism in trichoblasts is strong based on microtubule localization and inhibitors of polymerization (Seagull 1990; Tiwari and Wilkins 1995; Graham and Haigler 2021), cellulose-microfibril co-alignment

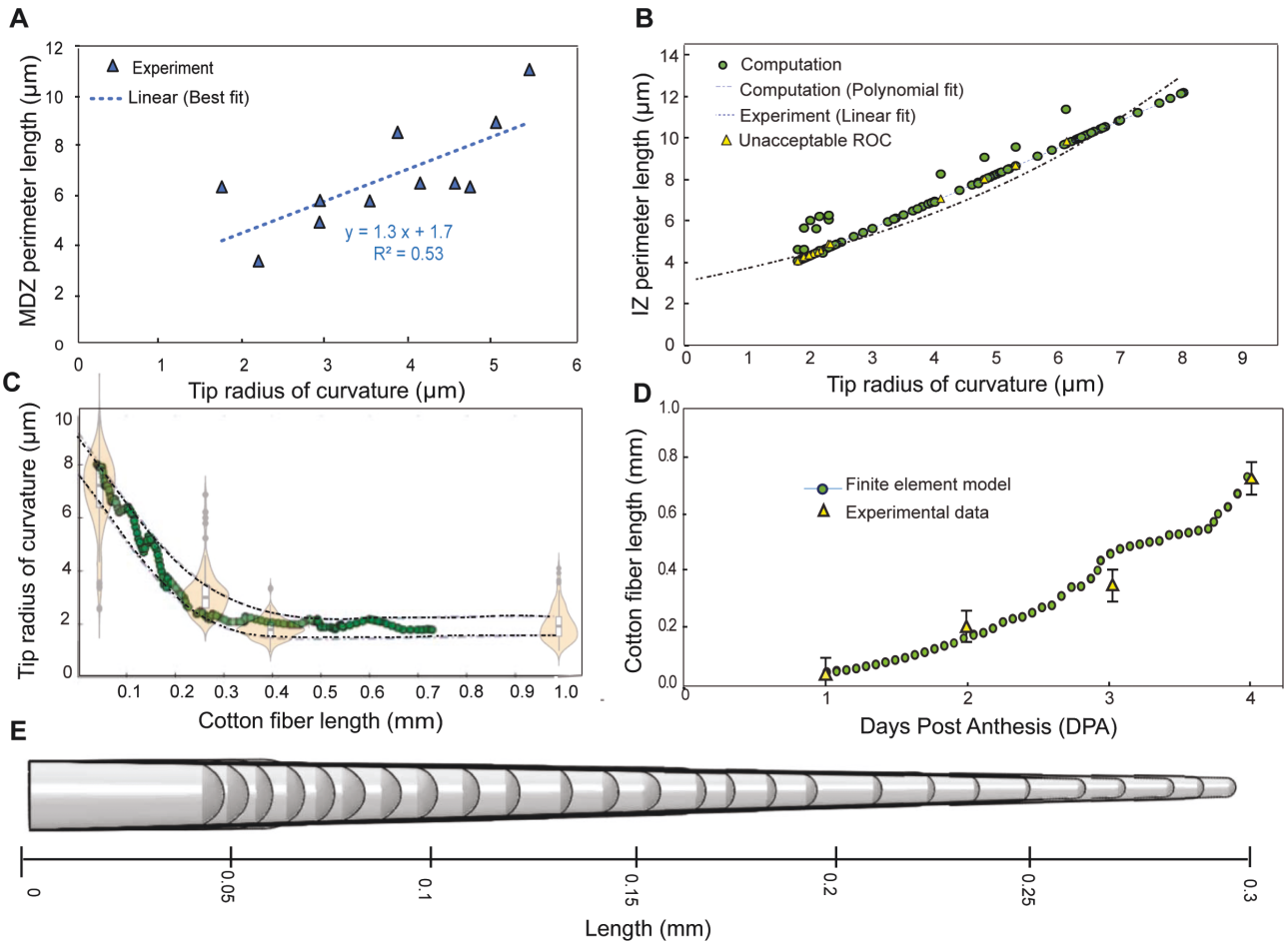

Figure 8. Tip radius of curvature (ROC) and microtubule depletion zone (MDZ): (A) Tapering of the cotton fibres from 1–4 DPA in the FE model is controlled by changing the IZ perimeter to be within the range defined by experimental data (shown in the background). IZ perimeter is based on the regression analysis of MDZ and tip radius of curvature measurements from the immunolocalization data described above. The resulting tapering is illustrated in (B) over the course of X modelling steps. (C) The ROC decreases in conjunction with a reduction of the MDZ perimeter during elongation. (D) The changes of IZ perimeter in the FE are consistent with the experimental data which is representative of appropriate assumptions in the FE model. (E) Comparison of the fibre length from the model in comparison with experimental data from Graham *et al.* (2021).

(Seagull 1992), the distributed pattern of new cell wall synthesis (Ryser 1977; Yanagisawa *et al.* 2015; Stiff and Haigler 2016), and the fact that fibre elongation rates (Graham and Haigler 2021), like those of leaf trichoblasts (Yanagisawa *et al.* 2015), increase as a function of fibre length. Our time-lapsed analysis of fibre growth and bead labelling data showed that cell expansion occurs distal to the fibre apex, and that growth rates may be faster toward the base at early growth stages (Fig. 1D and E). This appears to differ from Arabidopsis trichoblasts that also employ an anisotropic diffuse growth mechanism, but expand faster toward the tip because of a base-to-tip cell wall thickness gradient (Yanagisawa *et al.* 2015), which is not apparent in early stage cotton fibres (Fig. 7A, and see fig. 10 in Tiwari and Wilkins 1995). Quantitative analysis of the orientation of the microtubule network revealed a strong alignment of the cortical microtubule array at 90° to the long axis of the cell (Figs. 5 and 6). The 3D fibre model predicted the critical importance of a transverse fibre alignment along the shaft of the elongating cell (Fig. 9C and D). Local deviations from the transverse alignment of the fibres in the modelled cell generated local radial swelling. The predictions from the model are consistent with the variable types of swelling defects observed after exposure of growing fibres to microtubule-disrupting drugs on fibre shape (Seagull 1990; Tiwari and Wilkins 1995; Graham and Haigler 2021). Cell to cell variability in the types and extent of inhibitor-induced swellings is likely due to their poor accessibility to fibre surfaces that are buried in a dense mat of cells with hydrophobic character (Seagull 1990; Graham and Haigler 2021). Collectively our experimental data and simulation results indicate a strict requirement for an averaged orientation of microtubule-patterned microfibrils orthogonal to the growth axis. The alignment of microfibril bundles and lateral interactions between them generate a highly anisotropic wall that can resist radial swelling in

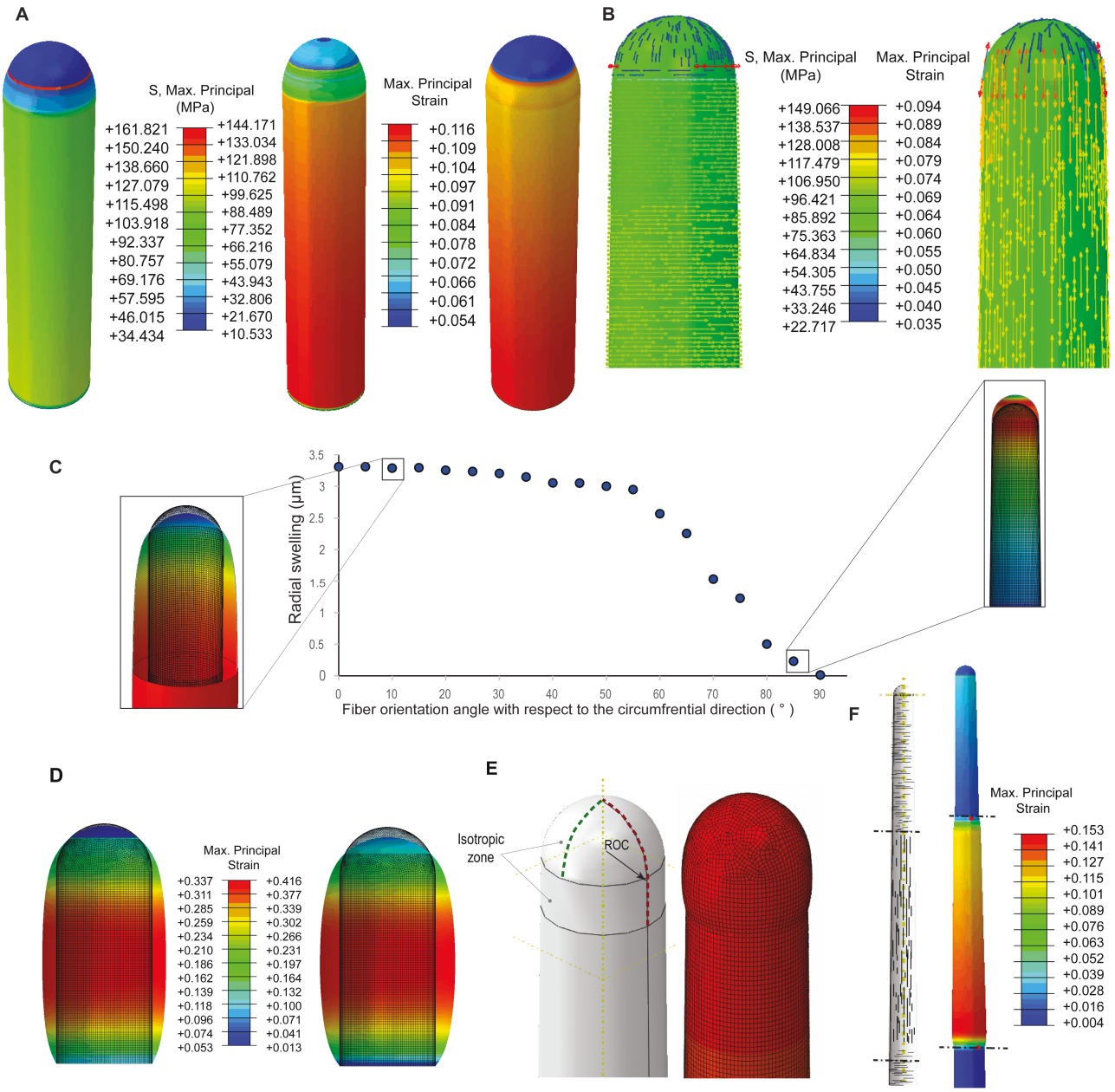

Figure 9. Spatial maps of stress and strain as a function of shape change. (A) The magnitudes of the maximum principal stress (MPa, left) with a sharp transition in material properties from the isotropic zone to the anisotropic shaft region and compared with (middle) a gradual transition from the isotropic tip to the anisotropic region. (Right) strain distribution in the gradual transition model. (B) Spatial orientation map of the maximum principal stress (MPa) and maximum principal strain in the gradual transition model in (A) with magnitude and orientation shown. (C) Changes in maximum principal stress with respect to cycle number of the growth model. ROC values at the apex are labelled at the top of the panel. Stress values were obtained at the fibre apex at the centre of the dome, at the shoulder of the dome 200 nm distal to the shoulder-shaft interface where the cell boundary becomes straight; shaft top: 100 nm proximal the shaft-shoulder interface; shaft bottom: 100 nm above the base.

the face ~100 MPa tensile forces (Zhang *et al.* 2021) that are similar in magnitude to those predicted here.

The above discussion is not intended to discount the central importance of the acto-myosin transport system during fibre morphogenesis. Cellulose fibres function within a pectin-rich matrix and their ratio as well as the overall thickness of the cell wall needs to be maintained as the fibre elongates. The maintenance of wall thickness and properties is an intrinsic and mechanism-free feature in the FE growth model

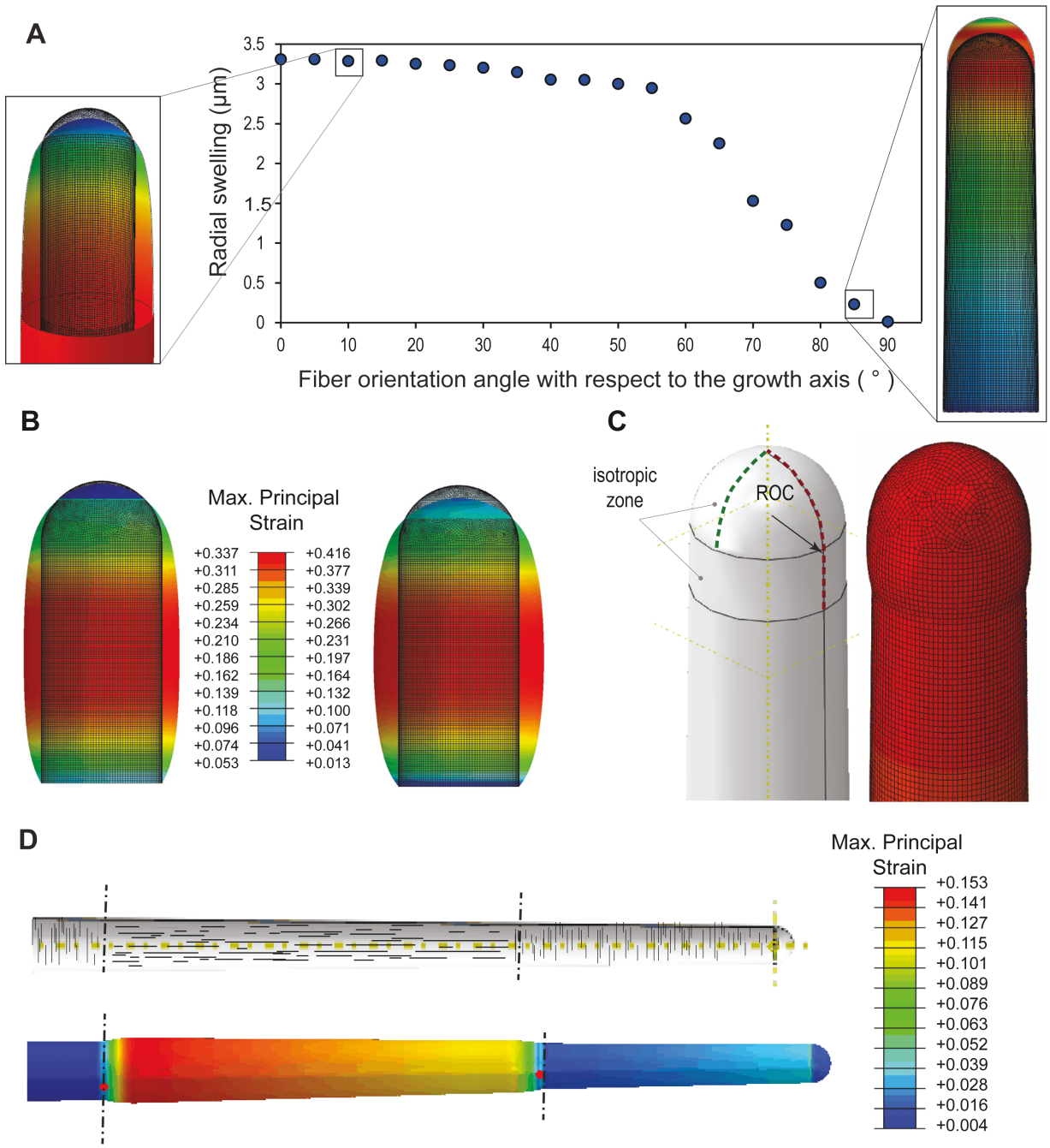

Figure 10. Sensitivity of cotton fibre expansion to orientation of cellulose microfibrils. (A) Sensitivity of expansion patterns to the orientation of cellulose microfibrils within the model relative to the longitudinal cell axis. (B) Maximum principal strain of 40 μm branches with CMFs aligned at 45° (left) and 0° (right) with respect to the longitudinal axis. (C) Sensitivity of tapering to the size of the isotropic tip zone of the fibre. Apical swelling occurs if the isotropic tip zone is extended (red dashed line) beyond the hemispherical dome (green dashed line). (D) Effects of a local intra-fibre domain of CMFs that are aligned with the fibre direction on strain magnitude and direction.

(Supplementary Information—Fig. S4), but in the cell this reflects the spatially controlled delivery of secretory vesicles and cargo that maintain wall thickness. In leaf trichoblasts, the actin system provides a coarse grain level of control over intracellular motility patterns and secretion activities that are needed to maintain cell wall thickness during growth (Yanagisawa *et al.* 2015), and we propose that a similar

mechanism operates in cotton fibers. Numerous genetic and actin localization studies point to the central importance of actin during fibre development and depict a network dominated by longitudinal bundles that are presumed to be involved in long-distance intracellular transport (Li *et al.* 2005; Wang *et al.* 2009; Bao *et al.* 2011b; Han *et al.* 2013; Lv *et al.* 2015; Yu *et al.* 2019). As expected, our phalloidin-staining protocol revealed prominent longitudinal bundles distributed within the fibre cytoplasm (Fig. 3; Supplementary Fig. 1).

We used a novel confocal live cell imaging approach using reflected, transmitted and fluorescent light signals to demonstrate the functionality of the actin bundle network to support longitudinal bidirectional flow along the fibre length (Fig. 4; Supplementary Information—Movies S1 and S2). In Arabidopsis trichoblasts, an actin-related protein (ARP)2/3-generated actin meshwork at the apex, that has only been detected with phalloidin, organizes the actin bundle network and bidirectional flow patterns in the growing branch (Yanagisawa *et al.* 2015). A live cell imaging analysis of actin in cotton fibres described tip signal as uniformly distributed 'fine actin filaments' (Yu *et al.* 2019). The published localization pattern could be explained by actin bundles that loop around the cell apex. Phalloidin staining clearly reveals tip actin meshworks in tapering leaf trichoblasts in Arabiodopsis (Le *et al.* 2003; Zhang *et al.* 2005; Yanagisawa *et al.* 2015) that are not detected as readily with live cell probes, probably because the GFP-tagged actin biosensors cannot gain physical access to the meshwork in live cells. We found no evidence for a cortical actin meshwork at the cotton fibre apex with phalloidin. The failure to detect a dense apical actin meshwork could be a fixation artefact; but plenty of individual actin filaments and bundles were detected in the apex albeit in different configurations. We may be proven wrong as more live cell imaging is done in cotton, but differences in actin architecture at the apex of trichoblasts are not completely unexpected. Leaf hairs taper to ~700 nm ROC, while cotton fibres hit a minimum ROC of more than 2.4 μm (Fig. 2). Cotton fibre tips either had a loose network of functional actin filament/bundle tracks that transited the fibre dome (Fig. 3A–C, Fig. 4D–H; Supplementary Information—Movie S4) or a population of longitudinal bundles that terminated along a distal ring just proximal to the cell apex. The actin bundle localization patterns are more consistent with the coupled actin polymerization and bundling activities of a Formin (Michelot *et al.* 2006; Vidali *et al.* 2009), rather than ARP2/3-generated meshworks (Yanagisawa *et al.* 2015). Perhaps the bundle-depleted apical zone observed in subsets of fibers reflects an oscillatory inhibition of actin polymerization or stability. This organization of roadways could lead to a more focused intracellular trafficking that enables pulsatile wall bending and growth at the apex.

4.2 Cytoskeletal and cell wall systems that enable fibre tapering

Fibre tapering is known to occur early in development (Stewart 1975; Butterworth *et al.* 2009) and the resulting decreased cell diameter underlies the trait of fibre fineness and the increased value of pima cotton and high thread count products. Fibre diameter is largely determined by 2 DPA in both *G. hirsutum* and *G. barbadense* fibres (Fig. 2), and in tapering cells the history of this shape change is recorded in the progressive reduction of cell diameter toward the cell apex. Once completed a stable cell diameter is propagated during an extended phase of cell elongation and 'self-similar' shape propagation until growth ceases after the transition to secondary wall synthesis is completed. Leaf trichoblasts use an isotropic tip zone in concert with highly anisotropic, tip-biased cell expansion to generate a fine-pointed cell that can deter insect feeding (Yanagisawa *et al.* 2015). In leaf hairs, the longitudinal growth rate gradient is not a form of tip growth, but instead reflects the effects of a longitudinal wall thickness gradient in the growing branch. ARP2/3-dependent patterning of the actin bundle system is required to coordinate cell wall thickness with growth, and the the failure to do explains many aspects of the *distorted* trichome phenotype. The isotropic tip zone is likely present because the apex lacks organized microtubules and cellulose fibre would be predicted to be randomly oriented in the dome. An MDZ with unique microtubule arrangements has been reported in cotton fibres at all stages of development (Szymanski and Staiger 2018; Graham and Haigler 2021) and in the leaf trichoblasts of multiple species (Beilstein and Szymanski 2004; Chang *et al.* 2019), suggesting that modulation of the geometry of IZ is an evolutionarily conserved cell shape control strategy.

Here an easily identifiable MDZ was detected in fibres at varying stages of the tapering process and the geometry of the MDZ is correlated with the apex radius of curvature (Figs. 5, 6, and 8A). The morphogenetic potency of the isotropic tip zone was established in a series of FE simulations with geometries and cell wall properties obtained from experimental data (Figs. 7B and 8E). Importantly when an adaptive growth model with a tunable IZ geometry was designed to use externally supplied values for isotropic tip zone size at each simulation cycle, it enabled the model to match the experimentally observed shape changes (Fig. 8; Supplementary Information—Fig. S4) with a non-linear tapering profile that mirrored the behaviours of living cells. Although the efficacy of isotropic tip zone-mediated tapering to explain the diverse phenotypes of *G. hirsutum* and *G. barbadense* fibres has been challenged (Graham and Haigler 2021), the simplest explanation is that all fibre cells use a similar tapering strategy and the observed variability is due to the differences among genotypes and individual cells in how efficiently the morphogenetic program is executed. The reproducibility of the tapering and fibre elongation process *in vivo* (Fig. 2) and the remarkable success with which adaptive FE models reproduce these behaviours (Fig. 8C–E, and Yanagisawa *et al.* 2015) strongly suggests that dynamic feedback controls integrate changes in apex cell wall geometry with the local behaviours of microtubule cytoskeleton. The magnitudes and directions of tensile forces that reflect the geometry of the cell and the compositional gradients of the wall may provide that link.

4.3 Wall stress, cell geometry and cellular-scale microtubule patterns

Our data indicate that cell wall stress patterns and cell geometry could go a long way toward explaining the cellular-scale patterns in the cortical microtubule array in tapering fibres. Correlations between mechanical stress in the cell wall and the organization of the cortical fibres and microtubules have been analysed for decades(Green 1962; Landrein and Hamant 2013), and numerous papers contain images in which microtubules are aligned with predicted tensile force patterns (Zandomeni and Schopfer 1994; Hejnowicz *et al.* 2000; Hamant *et al.* 2008; Jacques *et al.* 2013; Sampathkumar *et al.* 2014;

Belteton *et al.* 2021). However, methods to measure in-plane cell wall tensile forces in living cells do not exist, and most studies rely on qualitative stress predictions from FE models and single time-point microtubule imaging. In living cells, the microtubule network turns over completely in the time-scale of minutes and correlations among microtubule behaviours, wall stress and cell shape change are exceedingly difficult to detect (Wong *et al.* 2019; Beltetong *et al.* 2021). FE models with physiologically relevant turgor pressures (~1 MPa), realistic wall modulus values (~100 MPa), and a simulated middle lamellae predict that microtubule alignment responds to rather shallow spatial stress gradients and elevated stress correlates with increased local microtubule cortical occupancy (Belteton *et al.* 2021). The FE cotton fibre model here operates in plausible biomechanical regimes and enables one to generate realistic spatial maps of the stress. One limitation of the model is associated with the condition of full relaxation at each pressurization step which removed residual stresses in the wall. Future models without this constraint would allow the impact to be studied in more detail. In a refined model with smoothed material property transitions between the dome and shaft, there is a cellular-scale stress gradient with increasing values toward the fibre base (Fig. 9A and B). Stress is minimal in the apical dome, and if these local forces are near the threshold of a stress sensing mechanism that promotes polymerization, this could partially explain the existence of the MDZ.

The varying orientations of stress in the developing fibre cell may also contribute to cellular-scale microtubule patterning and the existence of an MDZ. Stress vectors in the apical dome are radially oriented toward the apex and orthogonal to those in the fibre shoulder and shaft (Fig. 9B). Cortical microtubules in the shoulder and shaft tend to be aligned with their co-localizing stress vectors transverse to the long axis of the cell, more persistent based their consistent detection, and more dense than those in the apex (Figs. 5 and 6). Transverse microtubules in the shoulder and flank are probably aligned further by shallow angle encounters between interacting microtubules (Dixit and Cyr 2004). As a result microtubules that polymerize from the apex toward the shoulder are more likely to experience elevated catastrophe rates because of steep angle encounters with the preexisting circumferential microtubules (Dixit and Cyr 2004). Plant cell expansion is slow occurring on the timescales of tens of minutes and the interface of these orthogonal stresses could specify a clean and stable circumferential boundary.

When coupled to a highly anisotropic fibre shaft, the apical MDZ and its encoded isotropic patch of wall is sufficient to cause tapering at the fibre apex. However, it was not clear how the cell might adaptively sense cell geometry to restrict the MDZ during tapering (Fig. 8C). Stress patterns could also function in this capacity. A growth simulation predicted that there are clear longitudinal gradients, with stress decreasing away from fibre apex (Fig. 9C). However, the gradient becomes dampened as the cell tapers largely because of the decreasing cell radius, and its sufficiency to pattern a progressively constricting MDZ seems doubtful. In contrast, the interface of orthogonal stresses near the apex/shoulder region is stable across the range of ROCs during tapering. A stress-patterned catastrophe inducing boundary modulated by signal transduction systems (Yanagisawa *et al.* 2015 & 2018) could provide a robust mechanism to link cell geometry with a morphologically potent MDZ.

Since microtubules can sense both the magnitude and direction of tensile forces, it seems most likely that some sort of transmembrane receptor links wall forces with microtubule organization (Williamson 1990). Computational simulations of microtubule dynamics indicate that coupling stress magnitude and direction to microtubule +-end dynamics is an effective mechanism to integrate cellular scale cortical arrays and cell geometry (Li *et al.* 2022). Given that the rate and degree of tapering are highly variable among genotypes, perhaps stress dependent microtubule patterning and localized intracellular signal transduction cascades operate in parallel to modulate cell wall properties and robustly define a constricting MDZ and reproducible growth outputs (Li *et al.* 2019).

4.4 Building a roadmap to cotton fibre engineering

Trichoblasts are the foundations of a global textile industry, an implement of plant defense against insect attack (Eisner *et al.* 1998), and a potential source of novel biomaterial products (Natalio *et al.* 2017). These single cell systems employ conserved morphogenesis control modules and are low-hanging fruit for trait engineering. In trichoblasts, cytoskeletal systems not only pattern the wall, but also appear to mediate feedback control from stress arrays that encode information reflecting both cell geometry and wall composition gradients. The degree of tapering varies between cell types and species; however, key cytoskeletal regulators of cell length and diameter likely have similar functions in Arabidopsis and cotton trichoblasts (e.g., Oppenheimer *et al.* 1997; Preuss *et al.* 2004). Therefore, there are broad opportunities to integrate knowledge and experimental approaches to fully leverage the predictive powers of FE modelling for trait engineering. Continued success will require collections of informative mutants, useful live cell marker lines, and quantitative time-lapsed imaging workflows. The associated multi-scale experimental data can be used to create FE models with realistic cytoplasmic inputs and feedback controls that can predict efficient strategies for cell shape engineering.

SUPPORTING INFORMATION

The following additional information is available in the online version of this article—

Movie S1. 5D reflected light and fluorescence time-lapse of bead-labeled cotton 1DPA fibers that were cultured in vitro. Tracks are the movement of the beads adhered to the fiber. Images were aligned relative to the long cell axis and bead number 1. Scale bar = 10μm.

Movie S2. 5D reflected and transmitted light imaging of a 2 DPA fiber prior to infusion of the media with Lat B.

Movie S3. 5D reflected and transmitted light imaging of the same cell as supplemental movie 2, but 5 minutes perfusion of the imaging chamber with Lat B.

Movie S4. 5D time lapsed imaging of transmitted and reflected light signals detecting curved trajectories of organelles that transit across the apex.

Figure S1. Longitudinal actin bundles are widely distributed in the fiber cytoplasm. **(A)** Projected images of the side view of a blunt fiber with a longitudinally aligned actin bundle network. White rectangle, region of image stack that was resliced in the y/z plane and projected in a'. **(B, C)** Example images of actin bundles in more tapered fibers that display distributed (A) and cortical (B) bundles. White rectangles and resliced projections are as in panel (A). Bars = 5 μm.

Figure S2. Three channel live cell imaging of a living 1 DPA cotton fiber. (**A**) Transmitted light image. (**B**) Reflected light image. (**C**) BCECF fluorescence of acidified vacuoles.

Figure S3. Additional example images of fibers at different degrees of tapering labeled with anti-tubulin antibodies and used to measure the perimeter of the MDZ as a function of tip radius of curvature. (**A to H**) In the paired sets of images the maximum projection of the cell is on the left and on the right are the same images including the ROIs that were used to measure radius of curvature and MDZ perimeter. Bars = 10 μm.

Figure S4. Flowchart of FE growth model of cotton fibers with ROC control. The green loop denotes the simulations without any need for MDZ perimeter readjustment. Minimum and maximum of ROC are defined according to the tapering of the cell wall from 1-6 DPA. The distance d is defined from the MDZ edge to the fiber tip by which each increment leads to an increase of MDZ perimeter and additional tapering.

ACKNOWLEDGEMENTS

Thanks to Rosemary White, Filomena Pettolino, and Phil Hands at the CSIRO Black Mountain lab who assisted with the live cell imaging experiments. TEM images were obtained with assistance from Dr. Chris Gilpin and Laurie Mueller at the Purdue Life Sciences Microscopy facility. Thank you to Thomas Davis for helping with the fibre tip morphology imaging. Thanks to Doris Kemmler and Candace Haigler for protocols and help establishing the ovule culture system. This work was supported by the National Science Foundation MCB grant no. 1715544 to D.B.S. and J.A.T. Cotton fibre live cell imaging was supported by the Purdue University as part of AgSEED Crossroads funding to D.B.S. Research conducted at CSIRO, Canberra, AU was done with support from the McKnight fellowship to D.B.S.

MODEL AND DATA AVAILABILITY

The example growth model shown in Fig. 8 is located in the repository folder 'InSilicoPlants_YanagisawaKeynia_2022' that is accessible for download at https://github.com/Turner-TULiPS.

AUTHORS' CONTRIBUTIONS

Conceptualization: D.B.S. and M.Y.; Methodology: M.Y., S.K. and S.B.; Investigation: M.Y., S.K. and S.B.; Validation: M.Y., S.K. and S.B.; Resources: D.B.S. and J.A.T.; Writing—original draft: D.B.S., M.Y., J.A.T. and S.K.; Writing—review and editing: D.B.S., M.Y., J.A.T., S.K. and S.B.; Visualization: D.B.S., M.Y., S.K. and S.B; Supervision: D.B.S. and J.A.T.; Project administration: D.B.S.; Funding acquisition: D.B.S. and J.A.T.

CONFLICT OF INTEREST STATEMENT

None declared.

REFERENCES

Ambrose C, Allard JF, Cytrynbaum EN, Wasteneys GO. 2011. A CLASP-modulated cell edge barrier mechanism drives cell-wide cortical microtubule organization in Arabidopsis. *Nature Communications* **2**:430.

Applequist WL, Cronn R, Wendel JF. 2001. Comparative development of fiber in wild and cultivated cotton. *Evolution & Development* **3**:3–17.

Bao Y, Hu G, Flagel LE, Salmon A, Bezanilla M, Paterson AH, Wang Z, Wendel JF. 2011a. Parallel up-regulation of the profilin gene family following independent domestication of diploid and allopolyploid cotton (*Gossypium*). *Proceedings of the National Academy of Sciences* **108**:21152–21157.

Bao Y, Hu G, Flagel LE, Salmon A, Bezanilla M, Paterson AH, Wang Z, Wendel JF. 2011b. Parallel up-regulation of the profilin gene family following independent domestication of diploid and allopolyploid cotton (Gossypium). *Proceedings of the National Academy of Sciences* **108**:21152–21157.

Baskin TI. 2005. Anisotropic expansion of the plant cell wall. *Annual Review of Cell and Developmental Biology* **21**:203–222.

Bassel GW, Stamm P, Mosca G, Barbier de Reuille P, Gibbs DJ, Winter R, Janka A, Holdsworth MJ, Smith RS. 2014. Mechanical constraints imposed by 3D cellular geometry and arrangement modulate growth patterns in the Arabidopsis embryo. *Proceedings of the National Academy of Sciences* **111**:8685–8690.

Basu D, El-Assal SE, Le J, Mallery EL, Szymanski DB. 2004. Interchangeable functions of Arabidopsis PIROGI and the human WAVE complex subunit SRA1 during leaf epidermal development. *Development* **131**:4345–4355.

Basu D, Le J, Zakharova T, Mallery EL, Szymanski DB. 2008. A SPIKE1 signaling complex controls actin-dependent cell morphogenesis through the heteromeric WAVE and ARP2/3 complexes. *Proceedings of the National Academy of Sciences* **105**:4044–4049.

Beilstein, M, Szymanski, D. 2004. Cytoskeletal requirements during *Arabidopsis* trichome development. In: Hussey P, eds. *The plant cytoskeleton in cell differentiation and development*. Oxford, UK: Blackwell, 265–289.

Belteton SA, Li W, Yanagisawa M, Hatam FA, Quinn MI, Szymanski MK, Marley MW, Turner JA, Szymanski DB. 2021. Real-time conversion of tissue-scale mechanical forces into an interdigitated growth pattern. *Nature Plants* **7**:826–841.

Boudon F, Chopard J, Ali O, Gilles B, Hamant O, Boudaoud A, Traas J, Godin C. 2015. A computational framework for 3D mechanical modeling of plant morphogenesis with cellular resolution. *PLoS Computational Biology* **11**:e1003950.

Butterworth KM, Adams DC, Horner HT, Wendel JF. 2009. Initiation and early development of fiber in wild and cultivated cotton. *International Journal of Plant Sciences* **170**:561–574.

Chang J, Xu Z, Li M, Yang M, Qin H, Yang J, Wu S. 2019. Spatiotemporal cytoskeleton organizations determine morphogenesis of multicellular trichomes in tomato. *PLoS Genetics* **15**:e1008438.

Chen X, Guo W, Liu B, Zhang Y, Song X, Cheng Y, Zhang L, Zhang T. 2012. Molecular mechanisms of fiber differential development between G. barbadense and G. hirsutum revealed by genetical genomics. *PLoS One* **7**:e30056.

Chickarmane V, Roeder AHK, Tarr PT, Cunha A, Tobin C, Meyerowitz EM. 2010. Computational morphodynamics: a modeling framework to understand plant growth. *Annual Review of Plant Biology* **61**:65–87.

Dixit R, Cyr R. 2004. Encounters between dynamic cortical microtubules promote ordering of the cortical array through

angle-dependent modifications of microtubule behavior. *Plant Cell* **16**:3274–3284.

Dyachok J, Shao M-R, Vaughn K, Bowling A, Facette M, Djakovic S, Clark L, Smith L. 2008. Plasma membrane-associated SCAR complex subunits promote cortical F-actin accumulation and normal growth characteristics in *Arabidopsis* roots. *Molecular Plant* **1**:990–1006.

Eisner T, Eisner M, Hoebeke ER. 1998. When defense backfires: detrimental effect of a plant's protective trichomes on an insect beneficial to the plant. *Proceedings of the National Academy of Sciences* **95**:441–444.

Evers JB. 2016. Simulating crop growth and development using functional-structural plant modeling. In: HKNÜ, AN, eds. *Canopy photosynthesis: from basics to applications advances in photosynthesis and respiration*. Dordrecht: Springer.

Fayant P, Girlanda O, Chebli Y, Aubin CE, Villemure I, Geitmann A. 2010. Finite element model of polar growth in pollen tubes. *Plant Cell* **22**:2579–2593.

Forouzesh E, Goel A, Mackenzie SA, Turner JA. 2013. In vivo extraction of Arabidopsis cell turgor pressure using nanoindentation in conjunction with finite element modeling. *The Plant Journal 73* **509**:520.

Fox S, Southam P, Pantin F, Kennaway R, Robinson S, Castorina G, Sanchez-Corrales YE, Sablowski R, Chan J, Grieneisen V, et al. 2018. Spatiotemporal coordination of cell division and growth during organ morphogenesis. *PLoS Biology* **16**:e2005952.

Graham BP, Haigler CH. 2021. Microtubules exert early, partial, and variable control of cotton fiber diameter. *Planta* **253**:47.

Green PB. 1962. Mechanisms for plant cellular morphogenesis. *Science* **138**:1404–1405.

Guimarães GC, Coelho Júnior MC, Garcia Rojas EE. 2009. Density and kinematic viscosity of pectin Aqueous solution. *Journal of Chemical & Engineering Data* **54**:662–667. doi:10.1021/je800305a

Haigler CH, Betancur L, Stiff MR, Tuttle JR. 2012. Cotton fiber: a powerful single-cell model for cell wall and cellulose research. *Frontiers in Plant Science* **3**:104.

Hamant O, Heisler MG, Jonsson H, Krupinski P, Uyttewaal M, Bokov P, Corson F, Sahlin P, Boudaoud A, Meyerowitz EM, et al. 2008. Developmental patterning by mechanical signals in *Arabidopsis*. *Science* **322**:1650–1655.

Hamant O, Inoue D, Bouchez D, Dumais J, Mjolsness E. 2019. Are microtubules tension sensors? *Nature Communications* **10**:2360.

Han LB, Li YB, Wang HY, Wu XM, Li CL, Luo M, Wu SJ, Kong ZS, Pei Y, Jiao GL, et al. 2013. The dual functions of WLIM1a in cell elongation and secondary wall formation in developing cotton fibers. *Plant Cell* **25**:4421–4438.

Hayot CM, Forouzesh E, Goel A, Avramova Z, Turner JA. 2012. Viscoelastic parameters of cell walls of single living plant cells determined by dynamic nanoindentation. *Journal of Experimental Botany* **16**:2525–2540. doi:10.1093/jxb/err428

Hejnowicz Z, Rusin A, Rusin T. 2000. Tensile Tissue Stress Affects the Orientation of Cortical Microtubules in the Epidermis of Sunflower Hypocotyl. *Journal of Plant Growth Regulation* **19**:31–44.

Horton P. 2000. Prospects for crop improvement through the genetic manipulation of photosynthesis: morphological and biochemical aspects of light capture. *Journal of Experimental Botany* **51**:475–485.

Hu G, Koh J, Yoo MJ, Pathak D, Chen S, Wendel JF. 2014. Proteomics profiling of fiber development and domestication in upland cotton (*Gossypium hirsutum* L.). *Planta* **240**:1237–1251.

Jacques E, Verbelen JP, Vissenberg K. 2013. Mechanical stress in Arabidopsis leaves orients microtubules in a 'continuous' supracellular pattern. *BMC Plant Biology* **13**:163.

Justus CD, Anderhag P, Goins JL, Lazzaro MD. 2004. Microtubules and microfilaments coordinate to direct a fountain streaming pattern in elongating conifer pollen tube tips. *Planta* **219**:103–109.

Kelly B, Abidi N, Ethridge D. 2015. Fiber to fabric. In: Fang DD, Percy RG eds. *Cotton*, 2nd edition. New York: Wiley, 665–744.

Keynia S, Davis TC, Szymanski DB, Turner JA. 2022. Cell twisting during desiccation reveals axial asymmetry in wall organization. *Biophysical Journal* **121**: 932–942. doi:10.1016/j.bpj.2022.02.013

Kierzkowski D, Runions A, Vuolo F, Strauss S, Lymbouridou R, Routier-Kierzkowska AL, Wilson-Sanchez D, Jenke H, Galinha C, Mosca G, et al. 2019. A growth-based framework for leaf shape development and diversity. *Cell* **177**:1405–1418.e17.

Kim HJ, Triplett BA. 2001a. Cotton fiber growth in planta and in vitro. Models for plant cell elongation and cell wall biogenesis. *Plant Physiology* **127**:1361–1366.

Kim HJ, Triplett BA. 2001b. Cotton fiber growth in planta and in vitro. Models for plant cell elongation and cell wall biogenesis. *Plant Physiology* **127**:1361–1366.

Landrein B, Hamant O. 2013. How mechanical stress controls microtubule behavior and morphogenesis in plants: history, experiments and revisited theories. *Plant Journal* **75**:324–338.

Le J, El-Assal SE, Basu D, Saad ME, Szymanski DB. 2003. Requirements for *Arabidopsis ATARP2* and *ATARP3* during epidermal development. *Current Biology* **13**:1341–1347.

Li XB, Fan XP, Wang XL, Cai L, Yang WC. 2005. The cotton ACTIN1 gene is functionally expressed in fibers and participates in fiber elongation. *Plant Cell* **17**:859–875.

Li W, Keynia S, Belteton SA, Afshar-Hatam F, Szymanski DB, Turner JA. 2022. Protocol for mapping the variability in cell wall mechanical bending behavior in living leaf pavement cells. *Plant Physiology* **188**: 1435–1449. doi:10.1093/plphys/kiab588

Li J, Kim T, Szymanski DB. 2019. Multi-scale regulation of cell branching: modeling morphogenesis. *Developmental Biology*. **451**:40–52.

Li S, Lei L, Somerville CR, Gu Y. 2012. Cellulose synthase interactive protein 1 (CSI1) links microtubules and cellulose synthase complexes. *Proceedings of the National Academy of Sciences of the United States of America* **109**:185–190.

Li J, Szymanski DB, Kim T-Y. *2022 Probing stress-regulated ordering of the plant cortical microtubule array via a computational approach*. doi:10.1101/2022.02.17.480928

Lockhart JA. 1965. An analysis of irreversible plant cell elongation. *Journal of Theoretical Biology* **8**:264–275.

Lv F, Wang H, Wang X, Han L, Ma Y, Wang S, Feng Z, Niu X, Cai C, Kong Z, et al. 2015. GhCFE1A, a dynamic linker between the ER network and actin cytoskeleton, plays an important role in cotton fibre cell initiation and elongation. *Journal of Experimental Botany* **66**:1877–1889.

Mariano M, El Kissi N, Dufresne A. 2014. Cellulose nanocrystals and related nanocomposites: Review of some properties and challenges. *Journal of Polymer Science Part B: Polymer Physics* **52**:791–806. doi:10.1002/polb.23490

Marc J, Granger CL, Brincat J, Fisher DD, Kao T, McCubbin AG, Cyr RJ. 1998. A GFP-MAP4 reporter gene for visualizing cortical microtubule rearrangements in living epidermal cells. *Plant Cell* **10**:1927–1940.

Meinert MC, Delmer DP. 1977. Changes in biochemical composition of the cell wall of the cotton fiber during development. *Plant Physiology* **59**:1088–1097.

Michelot A, Derivery E, Paterski-Boujemaa R, Guerin C, Huang S, Parcy F, Staiger CJ, Blanchoin L. 2006. A novel mechanism for the formation of actin-filament bundles by a nonprocessive formin. *Current Biology* **16**:1924–1930.

Natalio F, Fuchs R, Cohen SR, Leitus G, Fritz-Popovski G, Paris O, Kappl M, Butt HJ. 2017. Biological fabrication of cellulose fibers with tailored properties. *Science* **357**:1118–1122.

Oppenheimer DG, Pollock MA, Vacik J, Szymanski DB, Ericson B, Feldmann K, Marks MD. 1997. Essential role of a kinesin-like protein in *Arabidopsis* trichome morphogenesis. *Proceedings of the National Academy of Sciences* **94**:6261–6266.

Pang CY, Wang H, Pang Y, Xu C, Jiao Y, Qin YM, Western TL, Yu SX, Zhu YX. 2010. Comparative proteomics indicates that biosynthesis of pectic precursors is important for cotton fiber and Arabidopsis root hair elongation. *Molecular and Cellular Proteomics* **9**:2019–2033.

Paredez AR, Somerville CR, Ehrhardt DW. 2006. Visualization of cellulose synthase demonstrates functional association with microtubules. *Science* **312**:1491–1495.

Preuss ML, Kovar DR, Lee YR, Staiger CJ, Delmer DP, Liu B. 2004. A plant-specific kinesin binds to actin microfilaments and interacts with cortical microtubules in cotton fibers. *Plant Physiology* **136**:3945–3955.

Prusinkiewicz P, Runions A. 2012. Computational models of plant development and form. *The New Phytologist* **193**:549–569.

Puspoki Z, Storath M, Sage D, Unser M. 2016. Transforms and operators for directional Bioimage analysis: a survey. *Advances in Anatomy, Embryology, and Cell* **219**:69–93.

Qin YM, Zhu YX. 2011. How cotton fibers elongate: a tale of linear cell-growth mode. *Current Opinion in Plant Biology* **14**:106–111.

Qiu JL, Jilk R, Marks MD, Szymanski DB. 2002. The *Arabidopsis SPIKE1* gene is required for normal cell shape control and tissue development. *Plant Cell* **14**:101–118.

Renny-Byfield S, Gong L, Gallagher JP, Wendel JF. 2015. Persistence of sub-genomes in paleopolyploid cotton after 60 million years of evolution. *Molecular Biology and Evolution*: msv001.

Ryser U. 1977. Cell-wall growth in elongating cotton fibers—autoradiographic study. *Cytobiologie* **15**:78–84.

Santiago Cintrón M, Johnson GP, French AD. 2011. Young's modulus calculations for cellulose Iβ by MM3 and quantum mechanics. *Cellulose* **18**:505–516. doi: 10.1007/s10570-011-9507-1

Sampathkumar A, Krupinski P, Wightman R, Milani P, Berquand A, Boudaoud A, Hamant O, Jonsson H, Meyerowitz EM. 2014. Subcellular and supracellular mechanical stress prescribes cytoskeleton behavior in Arabidopsis cotyledon pavement cells. *eLife* **3**:e01967.

Seagull RW. 1990. The effects of microtubule and microfilament disrupting agents on cytoskeletal arrays and wall deposition in developing cotton fibers. *Protoplasma* **159**:44–59.

Seagull RW. 1992. Quantitative electron microscopic study of changes in microtubule arrays and wall microfibril orientation during *in vitro* cotton fiber development. *Journal of Cell Science* **101**:561–577.

Smithers ET, Luo J, Dyson RJ. 2019. Mathematical principles and models of plant growth mechanics: from cell wall dynamics to tissue morphogenesis. *Journal of Experimental Botany* **70**:3587–3600.

Stewart JM. 1975. Fiber initiation on the cotton ovule. *American Journal of Botany* **62**:723–730.

Stiff MR, Haigler CH. 2016. Cotton fiber tips have diverse morphologies and show evidence of apical cell wall synthesis. *Scientific Reports* **6**:27883.

Szymanski DB, Cosgrove DJ. 2009. Dynamic coordination of cytoskeletal and cell wall systems during plant cell morphogenesis. *Current Biology* **19**:R800–R811.

Szymanski DB, Marks MD, Wick SM. 1999. Organized F-actin is essential for normal trichome morphogenesis in *Arabidopsis*. *Plant Cell* **11**:2331–2347.

Szymanski DB, Staiger CJ. 2018. The actin cytoskeleton: functional arrays for cytoplasmic organization and cell shape control. *Plant Physiology* **176**:106–118.

Tiwari SC, Wilkins TA. 1995. Cotton (*Gossypium hirsutum*) seed trichomes expand via diffuse growing mechanism. *Canadian Journal of Botany* **73**:746–757.

Triplett BA. 2000. Cotton ovule culture: a tool for basic biology, biotechnology and cotton improvemnt. *In vitro Cellular and Developmental Biology* **36**:93–101.

Vidali L, van Gisbergen PA, Guerin C, Franco P, Li M, Burkart GM, Augustine RC, Blanchoin L, Bezanilla M. 2009. Rapid formin-mediated actin-filament elongation is essential for polarized plant cell growth. *Proceedings of the National Academy of Sciences* **106**:13341–13346.

Wang HY, Wang J, Gao P, Jiao GL, Zhao PM, Li Y, Wang GL, Xia GX. 2009. Down-regulation of GhADF1 gene expression affects cotton fibre properties. *Plant Biotechnology Journal* **7**:13–23.

Wasteneys GO, Willingale-Theune J, Menzel D. 1997. Freeze shattering: a simple and effective method for permeabilizing higher plant cell walls. *Journal of Microscopy* **188**:51–61.

Wendel JF, Brubaker CL, Seelanan T. The origin and evolution of *Gossypium*. In *Physiology of cotton*, Stewart JM, Oosterhuis D, Heithholt JJ, Mauney JR (eds.), Netherlands: Springer: 2010:1–18.

Wendel JF, Cronn RC. 2003. Polyploidy and the evolutionary history of cotton. *Advances in Agronomy* **78**:139–186.

Wendel JF, Olson P, DStewart JM. 1989. Genetic diversity, introgression, and independent domestication of old-world cultivated cottons. *American Journal of Botany* **76**:1795–1806.

Williamson RE. 1990. Alignment of cortical microtubules by anisotropic wall stresses. *Australian Journal of Plant Physiology* **17**:601–613.

Wong JH, Kato T, Belteton SA, Shimizu R, Kinoshita N, Higaki T, Sakumura Y, Szymanski DB, Hashimoto T. 2019. Basic proline-rich protein-mediated microtubules are essential for lobe growth and flattened cell geometry. *Plant Physiology* **181**:1535–1551.

Yanagisawa M, Alonso JM, Szymanski DB. 2018. Microtubule-dependent confinement of a cell signaling and actin polymerization control module regulates polarized cell growth. *Current Biology* **28**:2459–2466.

Yanagisawa M, Desyatova AS, Belteton S, Mallery EM, Turner JA, Szymanski DB. 2015. Patterning mechanisms of cytoskeletal and cell wall systems during leaf trichome morphogenesis. *Nature Plant* **1**:15014.

Yoo M-J, Wendel JF. 2014. Comparative evolutionary and developmental dynamics of the cotton (*Gossypium hirsutum*) fiber transcriptome. *PLoS Genetics* **10**:e1004073–e1004073.

Yu Y, Wu S, Nowak J, Wang G, Han L, Feng Z, Mendrinna A, Ma Y, Wang H, Zhang X, et al. 2019. Live-cell imaging of the cytoskeleton in elongating cotton fibres. *Nature Plants* **5**:498–504.

Zandomeni K, Schopfer P. 1994. Mechanosensory microtubule reorientation in the epidermis of maize coleoptiles subjected to bending stress. *Protoplasma* **182**:96–101.

Zang Y, Hu Y, Xu C, Wu S, Wang Y, Ning Z, Han Z, Si Z, Shen W, Zhang Y, et al. 2021. GhUBX controlling helical growth results in production of stronger cotton fiber. *iScience* **24**:102930.

Zhang X, Dyachok J, Krishnakumar S, Smith LG, Oppenheimer DG. 2005. IRREGULAR TRICHOME BRANCH1 in Arabidopsis encodes a plant homolog of the actin-related protein2/3 complex activator Scar/WAVE that regulates actin and microtubule organization. *Plant Cell* **17**:2314–2326.

Zhang C, Mallery E, Reagan S, Boyko VP, Kotchoni SO, Szymanski DB. 2013. The endoplasmic reticulum is a reservoir for WAVE/SCAR regulatory complex signaling in the Arabidopsis leaf. *Plant Physiology* **162**:689–706.

Zhang Y, Yu J, Wang X, Durachko DM, Zhang S, Cosgrove DJ. 2021. Molecular insights into the complex mechanics of plant epidermal cell walls. *Science* **372**:706–711.

Zsivanovits G, MacDougall AJ, Smith AC, Ring SG. 2004. Material properties of concentrated pectin networks. *Carbohydrate Research* **339**:1317–1322. doi: 10.1016/j.carres.2004.02.027